Spatial Dynamics of Steady Flames 2. Low-Dimensional Manifolds and the Role of Transport Processes

Michael J. Davis*,† and Alison S. Tomlin‡

Chemical Sciences and Engineering Division, Building 200, Argonne National Laboratory, Argonne, Illinois 60439, and School of Process, Environmental, and Materials Engineering, University of Leeds, Leeds, United Kingdom

Received: February 15, 2008; Revised Manuscript Received: April 29, 2008

The study of the spatial dynamics of steady one-dimensional H_2/O_2 flames is continued. Algorithms for generating low-dimensional manifolds for these systems are presented and used to find low-dimensional manifolds for the flames and the corresponding adiabatic, isobaric chemical-kinetic systems. It is demonstrated that these algorithms generate manifolds that are more accurate than the ILDM algorithm for two-dimensional manifolds of the flames. The manifolds are then employed to study the relationship between the manifolds of the flame and the manifolds of the chemical-kinetic system. It is shown that the one-dimensional manifolds of the flame match well with the composite manifolds of the chemical kinetics, but that for two-dimensional manifolds there are discrepancies between the flame manifolds and the chemical-kinetic manifolds.

I. Introduction

In our previous Article, the spatial dynamics of steady H_2/O_2 flames were studied in detail[1] using the dynamical-system formulation of Hirschfelder and Curtiss[2] and Dixon-Lewis.[3] It was shown in ref 1 that steady flames were trajectories on a stable manifold of a saddle fixed point. This saddlepoint corresponds to a chemical equilibrium, but is unstable due to transport processes. The goal of that study was to understand the phase space structure of flame systems, and this led to the conclusion that there were attractive low-dimensional submanifolds on the stable manifold of the saddlepoint. An important result from ref 1 was that the dimension of the stable manifold matches the dimension of the adiabatic, isobaric chemical-kinetic system under most conditions. This makes the comparison between the chemical-kinetic systems and the flame systems more straightforward.

Because the accurate modeling of reactive flows is computationally intensive,[4] there has been a good deal of interest in finding means to reduce the effort, reviewed in several places.[5] The need for reduction is particularly acute, because these systems are multiscale in nature, with a large range of spatio-temporal scales. One means for accomplishing this reduction is through the use of low-dimensional manifolds. Important work by Maas and Pope,[6] Fraser, Roussel, and co-workers,[7–10] and Lam and Goussis[11] examined the phenomenology that leads to low-dimensional manifolds and presented important methods for reducing the dimension of systems based on this realization. Many other workers have examined and extended these methods.[5,12–25] The mathematical foundations of the methodologies have also been elucidated.[26–28]

The effect of transport processes on reduction has been studied for several years,[12–14,18–23,29] and this Article is a contribution to that field. Its main goal is to examine and understand the relationship between low-dimensional manifolds of chemical-kinetic systems without transport and manifolds of one-dimensional flames with the same chemical kinetics but also transport processes. This study is done within a dynamical-systems perspective, something that was undertaken previously for chemical-kinetic systems in ref 15, and one important aspect of the Article is to devise means to compare the spatial dynamics of flames with the temporal dynamics of corresponding chemical-kinetic systems through the low-dimensional manifolds.

Part 1 (our previous Article) showed numerical evidence that there were low-dimensional submanifolds of the stable manifold of the saddlepoint of the flame. The purpose of this Article is to continue that study by explicitly generating one- and two-dimensional manifolds. This Article will have a detailed comparison of the flame manifolds with the chemical-kinetic manifolds and will demonstrate that for one-dimensional manifolds there is little difference between the flame manifolds and composites of the chemical-kinetic manifolds, but that there are differences between the two types of two-dimensional manifolds. Comparisons will also be made between the more accurate manifolds generated here and ILDMs.[6] It will be shown that the ILDMs are accurate for one-dimensional manifolds, but not for two-dimensional manifolds.

The outline of this Article is as follows. Section II describes the generation of low-dimensional manifolds. Section III presents several numerical examples of one- and two-dimensional manifolds for a chemical-kinetic system and a flame system. It also presents comparisons of the manifolds generated in this Article and the more approximate ILDMs. Section IV presents the main results of the Article, comparing the low-dimensional manifolds of the flame systems and composite low-dimensional manifolds generated from adiabatic, isobaric chemical kinetics. Section V presents further results, showing how these comparisons vary with stoichiometry and enthalpy. Section VI has further discussions and conclusions.

* Corresponding author. E-mail: davis@tcg.anl.gov.
† Argonne National Laboratory.
‡ University of Leeds.

10.1021/jp801370p CCC: $40.75
Published on Web 08/07/2008

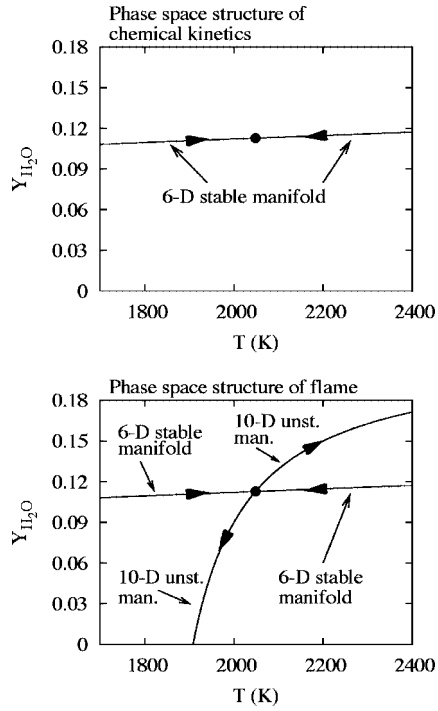

Figure 1. The phase space structure of a chemical-kinetic system is shown in the top panel, and the phase space structure of a flame system is shown in the bottom panel. Y_{H_2O} refers to the mass fraction of H_2O.

II. Low-Dimensional Manifolds

A. Background. Reference 1 studied the detailed dynamics of steady flames from a dynamical-systems perspective using the formulation of refs 2 and 3. It was shown that a steady flame was a trajectory on the stable manifold of a saddle fixed point. This fixed point corresponds to an equilibrium point of an adiabatic, isobaric system. The instability arises due to the transport equations, as the stable manifold is generally the same dimension as the chemical-kinetic space. Figure 1 summarizes the phase space structure of a system governed by adiabatic, isobaric conditions as compared to the flame system studied in ref 1 and here.

The top panel indicates that an adiabatic, isobaric system is stable. In this case, the stable manifold for the H_2/O_2 system[30] is at least as large as the space of all physically realizable chemical species and temperature.[12] The long-time behavior of any trajectory started on the stable manifold is to approach the equilibrium point, as indicated by the arrows on the stable manifold in the top panel.

The flame system is unstable, as shown in the bottom panel of Figure 1. For almost all cases we have studied, the 16-dimensional phase space of the flame system has a 6-dimensional stable manifold and a 10-dimensional unstable manifold. In addition, the sum of the eigenvalues of the Jacobian of the system at the saddlepoint is greater than zero, making the system a repellor.[31] An arbitrary trajectory will have components on both the stable and the unstable manifolds. This means that an arbitrary trajectory of the system will not eventually be attracted to the saddlepoint, but will generally move to infinity at long time, or perhaps to a sink outside the physical region. In ref 1, a simple example of such unstable behavior was presented and summarized in Figure 7 there. The instability of the flame dynamics is well-known[32] and led to the development of numerical procedures involving the solution of the steady flame problem based on second-order differential equations and boundary-value techniques that are more stable than methods that rely on the integration of trajectories of the unstable dynamical system shown in the bottom panel of Figure 1. An example of such a code is "Premix" in the Chemkin package.[32,33]

Reference 1 also studied the dynamics of the H_2/O_2 system of ref 30 away from the saddlepoint. Numerical evidence was presented in ref 1 that suggested the stable manifold pictured in the bottom panel of Figure 1 extended away from the saddlepoint and that the separation of spatial scales on the stable manifold evident near the saddlepoint extended well away from the saddlepoint. The present study extends the observations of ref 1 by explicitly generating one- and two-dimensional manifolds that are submanifolds of the six-dimensional stable manifold. Of particular interest in this Article is how the submanifolds of the stable manifold of the flames compare to the low-dimensional manifolds of the adiabatic, isobaric chemical-kinetic system, whose dynamics is presented near its equilibrium in the top panel of Figure 1.

B. Generating Low-Dimensional Manifolds. Using a modification of the ILDM algorithm of Maas and Pope,[6] Bongers et al.[19] demonstrated that it was possible to estimate submanifolds of a stable manifold using techniques originally developed for stable systems. The goal of ref 19 was to explore the possibility of improving ILDMs for reactive flow problems by calculating them with diffusion included. They found that the manifolds calculated this way for steady flames outperformed manifolds estimated only from chemical kinetics. The nature of the present study is exploratory, and it takes a somewhat different approach than does ref 19. The low-dimensional submanifolds are calculated for the flame systems with full transport, and direct comparisons are made to chemical-kinetic manifolds. Although the ILDM algorithm is generally not used in this Article, comparisons are made to manifolds generated from that algorithm in section III.C.

Low-dimensional manifolds are calculated here using Fraser's algorithm.[7–18] References 15 and 17 provide numerical procedures for the implementation of this method. A system of first-order equations defines a dynamical system:

$$\frac{dy_m}{dx} = F_m, m = 1 \rightarrow n \tag{2.1a}$$

where it is assumed that the independent coordinate is the spatial coordinate x, which it is for the flame. For the chemical-kinetic cases studied here, the independent coordinate is time. There are n equations describing n dependent coordinates that are indexed by the integer m. The dynamical system defined by eq 2.1a is described as "n-dimensional". For the flame system studied here and in ref 1, $n = 16$, with the 16 y_m's referring to 9 mol fractions (X_k), 6 mass flux fractions (G_k), and the temperature (T). The dimension is 16 rather than 21 (10 X's, 10 G's, and T) because the X's and G's sum to 1.0 and there are three additional constants associated with the mass flux fractions. In all calculations, the y's refer to the following:

$$y_m, m = 1 \rightarrow 9, X_{O_2}, X_H, X_O, X_{OH}, X_{HO_2}, X_{H_2O_2}, X_{Ar}, X_{He}, X_{H_2O}$$

$$y_m, m = 10 \rightarrow 15, G_H, G_O, G_{OH}, G_{HO_2}, G_{H_2O_2}, G_{H_2O}$$

$$y_{16} = T \tag{2.1b}$$

The other five coordinates, X_{H_2}, G_{H_2}, G_{O_2}, G_{Ar}, G_{He}, are calculated from the constants noted above and described in ref 1.

The algorithm for calculating manifolds starts by writing the equation for an M-dimensional manifold based on eq 2.1a:

$$F_m(\{y\},\{z\}) = \sum_{j=1}^{M} \frac{\partial y_m}{\partial z_j} F_j(\{y\},\{z\}), \{z\} \cap \{y\} = \emptyset \tag{2.2a}$$

where it is assumed that a subset of the original coordinates, labeled as $\{z\}$, can be used as a good coordinate system along the manifold. It may be necessary to take a more general coordinate system for the manifold under some circumstances, but that does not appear to be the case for the systems studied here. For the manifolds studied here, the following are used for the manifold coordinates:

$$\text{1D manifolds: } z_1 = y_{16} \equiv T$$

$$\text{2D manifolds: } z_1 = y_{16} \equiv T,\ z_2 = y_{15} \equiv G_{H_2O} \tag{2.2b}$$

Subtraction of the left- and right-hand sides of eq 2.2a leads to the following form of the manifold equations that is used for numerical solutions:

$$F_m(\{y\},\{z\}) - \sum_{j=1}^{M} \frac{\partial y_m}{\partial z_j} F_j(\{y\},\{z\}) = 0 \tag{2.2c}$$

In this Article, one-dimensional manifolds are generated with temperature as z for the chemical-kinetic systems. For two-dimensional manifolds, the z's are T and Y_{H_2O} for the chemical-kinetic systems (eq 2.1a in ref 1).

Fraser's algorithm is used because it is more accurate for two-dimensional manifolds in the flame system than the less computationally intensive algorithm of Maas and Pope,[6] a situation encountered previously for two-dimensional manifolds in large systems in ref 23b, where significant error analysis was undertaken. References 10, 15, 18, and 26 also have error analysis of the Maas−Pope algorithm. A significant modification is made to the version of Fraser's algorithm developed in ref 15, which is now described.

The algorithm starts with an initial guess and allows the system to relax to a slow manifold. In previous work using numerical techniques,[15,17] the initial guess was the Maas−Pope ILDM. In the present Article, the initial guesses are linear manifolds emanating from the equilibrium point of the chemical-kinetic systems or the submanifolds of the stable manifold of the saddlepoint of the flame systems.

Equation 2.2c is solved on a discrete grid as in ref 15. For one-dimensional manifolds, the grid is labeled with a single index and uses the independent variable z_1. If the grid points are labeled with the index k and there are N points on the grid, the following set of $(n-1) \times N$ coupled equations result:

$$S_{km} = \Delta z_{kl} F_{km} - \Delta y_{km} F_{kj} = 0, m = 1 \rightarrow n, k = 1 \rightarrow N, m \neq j \tag{2.3}$$

where the grid is not necessarily defined with even increments in z_1, the independent coordinate along the manifold, which is assumed to be y_j in eq 2.3, as defined in eqs 2.1b and 2.2b.

Two-dimensional manifolds are defined on an $N \times M$ grid with indices k and r. The function S is defined at each grid point for each species in the following discrete form of eq 2.2c:

$$S_{krm} = \Delta z_{kr1} \Delta z_{kr2} F_{krm} - \Delta y_{kpm} \Delta z_{kr2} F_{krj} - \Delta y_{rjm} \Delta z_{kr1} F_{krp} = 0,$$
$$m = 1 \rightarrow n,\ m \neq j,p,\ k = 1 \rightarrow N,\ r = 1 \rightarrow M \tag{2.4}$$

The grid in eq 2.4 is not necessarily defined with even increments in z_1 and z_2, the independent coordinates that are defined in eq 2.2b. Equation 2.4 describes $(n-2) \times N \times M$ coupled equations.

Equations 2.3 and 2.4 describe the general equations, which are solved for one-dimensional and two-dimensional manifolds. Equation 2.2b defines the independent coordinates z_1 and z_2, and eq 2.1b defines all of the coordinates (y's) in terms of their original designations.

Reference 15 described a relaxation procedure to converge eqs 2.3 and 2.4, but it was used only for one-dimensional manifolds. The method was modified in ref 17 and extended to the calculation of two-dimensional manifolds. A new version of the algorithm of ref 15 is developed here that involves two relaxation procedures and is different from the algorithms in refs 15 and 17.

As in ref 15, the relaxation procedure starts with a Newton−Raphson approach to solving for the y's in eqs 2.3 and 2.4. In the usual manner,[34] a Jacobian is defined for the S's in terms of the y's. This Jacobian leads to a system of linear equations:

$$\mathbf{J}_S^{\mathbf{P}}(\mathbf{y}-\mathbf{y}') = \mathbf{S}_{kr} \tag{2.5}$$

The superscript "P" in eq 2.5 indicates that $\mathbf{J}_s^{\mathbf{P}}$ is evaluated pointwise on the grid. This means that $\mathbf{J}_s^{\mathbf{P}}$ is an $(n-1) \times (n-1)$ matrix for one-dimensional manifolds and an $(n-2) \times (n-2)$ matrix for two-dimensional manifolds. The vectors $\mathbf{y}$, $\mathbf{y}'$, and $\mathbf{S}_{kr}$ have length $n-1$ for one-dimensional manifolds and $n-2$ for two-dimensional manifolds. The vectors $\mathbf{y}$, $\mathbf{y}'$ are the old guess and the new guess, respectively. Equation 2.5 is solved with the Lapack routines dgetrf and dgetrs.[35] Following ref 15, a pseudotime step is defined, and the following set of equations is solved with a fourth-order Runge−Kutta algorithm:

$$\frac{d\mathbf{y}}{d\tau} = \mathbf{y}-\mathbf{y}' \tag{2.6}$$

The Runge−Kutta vector on the right-hand side of eq 2.6 has length that reflects the size of the grid and the number of species. For example, for one-dimensional manifolds, its length is $(n-1) \times N$, where n refers to the number of species (including temperature) and N refers to the number of points along the one-dimensional grid. The relaxation procedure requires the solutions to a series of linear equations as outlined in eq 2.5. For example, a one-dimensional manifold solved on a grid of 50 points along the temperature variable requires 50 solutions to eq 2.5 with length $(n-1)$, and a 50×50 2-D grid requires the solution of 2500 linear systems of length $(n-2)$. This relaxation procedure is terminated under two conditions, a minimum tolerance is reached for the maximum value of $\Delta y_k = y_k - y'_k$ or the procedure does not converge evenly:

$$|(y_k - y'_k)|(\tau + \Delta\tau) > |(y_k - y'_k)|(\tau) \tag{2.7}$$

The results of the initial relaxation procedure are then used as input to a second relaxation procedure that depends on the full extent of the manifold. A damped Newton−Raphson[34] method is used in this case. Equation 2.5 has the same form:

$$\mathbf{J}_s^{\mathbf{f}}(\mathbf{y}-\mathbf{y}') = \mathbf{S}_{kr} \tag{2.8}$$

$\mathbf{J}_s^{\mathbf{P}}$ is a matrix generated by varying all points on the grid for all species. A damped version of eq 2.8 signifies that the updated version of $\mathbf{y}$ on the kth iteration is not $\mathbf{y}'$ but a vector that lies between the $(k-1)$th iterate of $\mathbf{y}$ and $\mathbf{y}'$:

$$\mathbf{y}^{(k)} = \mathbf{y}^{(k-1)} + \Delta\tau(\mathbf{y}' - \mathbf{y}^{(k-1)}) \quad (2.9)$$

The vectors $\mathbf{y}$, $\mathbf{y}'$, and $\mathbf{S_{kr}}$ have length $(n-1) \times N$ for one-dimensional manifolds and $(n-2) \times N \times M$ for two-dimensional manifolds defined on an NxM grid. Because of the larger number of points, the solution of eq 2.8 is much more computationally difficult than the initial relaxation procedure. However, the Jacobian matrix in eq 2.8 is sparse for two-dimensional manifolds, and sparse linear algebra techniques can be used[36] to reduce the computational effort. The sparse system solver "super LU"[37] is used to solve eq 2.8 for two-dimensional manifolds. Once again, as in the case of the first relaxation procedure, convergence is assumed when the maximum component of $\mathbf{S}$ in eqs 2.2a and 2.3 is less than a given tolerance. It is assumed that the procedure is not converged if convergence is not uniform in the sense of eq 2.7.

These methods have been tested for a large number of chemical-kinetic and flame systems, over the range of parameters plotted in Figure 12 and Figure 13 of ref 1. These tests are now summarized for the flame of ref 1 (see Figure 16 there).

C. One-Dimensional Manifolds. A result for the relaxation procedure outlined above is presented for the standard flame system of ref 1 presented in Figures 16−19 there. In this way, a manifold is generated that includes full transport. An analogous calculation has also been done for the chemical-kinetic version of this system, with similar results obtained, but not presented in this Article. The results presented in Figure 2 are representative of a series of results generated for the set of systems illustrated in Figure 13 of ref 1 and sampled in section V.

The independent variable (z above) is always chosen to be temperature. The top panel of Figure 2 shows a series of calculations that start relatively close to the saddlepoint and work away from it. The saddle is at $T = 2048$ K, and a linear segment is extended to $T = 1600$ K. This initial segment is converged with the double relaxation method described above. There are a total of 50 points used to estimate the manifold. This segment is then extended 20 K by adding a point at the end that is estimated by extrapolation. The additional 49 points along the manifold are chosen to lie along the previous manifold estimate by interpolating from the 50 points used in the previous segment.

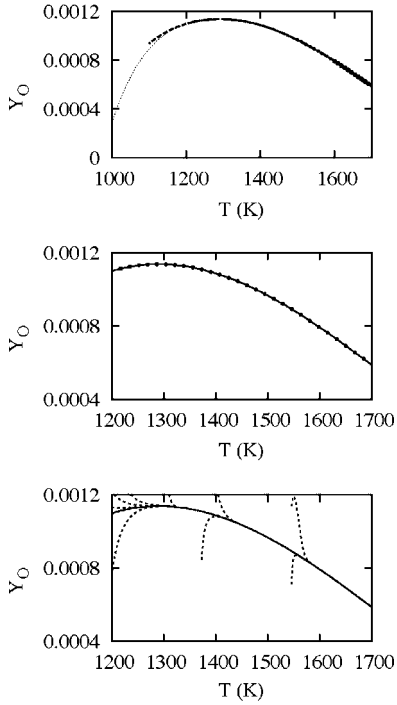

Figure 2. A series of one-dimensional manifolds are estimated in the top panel as described in the text. Large dots show the estimate out to 1600 K, small dots to 1500 K, the segment out to 1400 K is a thick dashed line, the segment to 1300 K is a thick solid line, the one to 1200 K is a dashed−dotted line, the segment to 1100 K is a thick dashed line, and the one to 1000 K is a thin dotted line. The middle panel compares the incremental convergence of the manifold out to 1200 K from the top panel as a solid line, and a series of dots show the direct calculation of the manifold. The bottom panel demonstrates that trajectories are attracted to the manifold.

The procedure is extended out to 1000 K if possible, as it is for the calculation here. We have found many situations where convergence out to 1000 K cannot be achieved in the uniform manner described above and the calculation is stopped at the temperature where uniform convergence cannot be achieved. All calculations for the parameter ranges shown in Figure 13 of ref 1 can be converged down to at least 1200 K.

The top panel of Figure 2 shows a series of seven of these calculations with end points at 1600 to 1000 K in 100 K increments. The figure caption describes how each of these calculations is plotted. This panel demonstrates that the manifold is converged out to approximately 1200 K, because all manifolds down to 1000 K are the same through 1200 K. It demonstrates that the manifolds diverge after that. These results are typical for a wide range of stoichiometries and asymptotic enthalpies, and it is assumed in the rest of this Article that one-dimensional manifolds can be converged to 1200 K, but not necessarily lower.

This Article compares manifolds. One set of comparisons is between chemical-kinetic manifolds and flame manifolds, and another is between manifolds generated with two different algorithms. So it is desirable to have portions of the manifold for which convergence is not in doubt. As demonstrated in the top panel of Figure 2, it is possible to use the algorithm below 1200 K, but it is not clear that algorithm is properly converged, for the reasons discussed above. In addition, ref 1 has several figures showing the manner in which the flame and chemical-kinetic systems relax, and it is clear that any portion of the one-dimensional manifold that extends below 1200 K is highly unattractive. Because of this discussion, we chose a convergence procedure that provides conservative estimates of the extent of the one-dimensional manifolds to make sure that any differences observed in the comparisons were accurate.

The middle panel of Figure 2 compares the incremental calculation of the top panel with the direct calculation of the manifold from a linear segment extended all the way out to $T = 1200$ K. The solid line shows the results of the incremental calculation from the top panel, and the dots show the results of the convergence of the algorithm for an initial linear segment extended out to 1200 K. This plot demonstrates that the direct calculation is sufficiently accurate and will allow for a simpler comparison between the chemical-kinetic and flame manifolds discussed below.

The bottom panel of Figure 2 repeats the one-dimensional manifold from the middle panel and also includes trajectories drawn as dashed lines. The plot demonstrates that trajectories are attracted to the one-dimensional manifold. As discussed in ref 1, these trajectories are on the stable manifold, and such trajectories cannot generally be propagated directly with numerical integration, because any error in their initial conditions causes them to be propagated to infinity along the unstable manifold. Reference 1 presented an algorithm for generating such trajectories, and this is what was used to calculate the trajectories in the bottom panel of Figure 2.

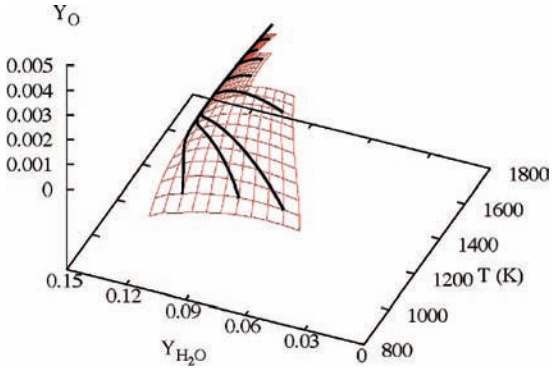

Figure 3. An example of a two-dimensional manifold is shown. It is constructed from three pieces, as described in the text. Eight trajectories were generated with initial conditions on the manifold, and the plot demonstrates that they stay on the manifold. The temperature ranges of the three overlapping pieces used to construct the manifold are 800−1200, 1250−1500, and 1450−1700 K.

D. Two-Dimensional Manifolds. The finite extent observed for one-dimensional manifolds in the previous subsection also causes difficulties in estimating two-dimensional manifolds (it is the same issue but in a different part of phase space). The two coordinates used to describe the manifold for the flame systems are temperature and the mass flux fraction of water, G_{H_2O} (eqs 2.2a−c). It was found that two-dimensional manifolds in the flame systems get narrower in the coordinate G_{H_2O} as they approach the saddlepoint. Because of this, various techniques were explored to change the boundary of the manifold as it approached the saddlepoint. These techniques are still under development, and instead it was decided to generate the manifold in three overlapping sections whose width in G_{H_2O} was constant along each piece, but got narrower as the sections got closer to the saddlepoint. On the basis of a comparison with trajectories, it was found that these provided good estimates of the manifold, provided that the portions had at least a length of 100 K in temperature. The overlap of the pieces provides a check for convergence of each of the pieces.

Because the manifolds are so narrow near the saddlepoint, it was decided that the manifolds would only be generated to $T = 1700$ K or $T = 1800$ K. The one-dimensional manifold is highly attractive above this temperature, making analysis of the two-dimensional manifold of less relevance. It was also found that the two-dimensional manifolds rarely could be converged below 800 K, and this led to the following ranges of temperatures used in the calculations: 800(850)−1250, 1200−1500, and 1450−1700(1800) K. There are two ranges listed for the lowest temperature portion, because the two-dimensional manifolds for lean flames generally did not extend below about 850 K. For stoichiometric and rich flame systems, they can generally be extended down to 800 K. Convergence was achieved in the manner described in section II.A by changing the boundary in the coordinate G_{H_2O} for the temperature ranges designated. All of the results presented in the Article were generated for manifolds calculated from three pieces converged on an 11 × 11 grid. Grid size was increased for all of the manifolds presented here, and the results did not change in a significant way.

Figure 3 shows a two-dimensional manifold generated with the algorithm discussed in this subsection and section II.A. Note how the manifold gets narrow for each of the three pieces as the temperature increases along the manifold. Note also how the pieces fit smoothly together, which is an indication of the convergence. The solid lines drawn on the manifold provide another indication of the convergence of the algorithm. These are trajectories that were started on the manifold and stay on the manifold throughout their propagation, an indication of the invariance of the manifold.

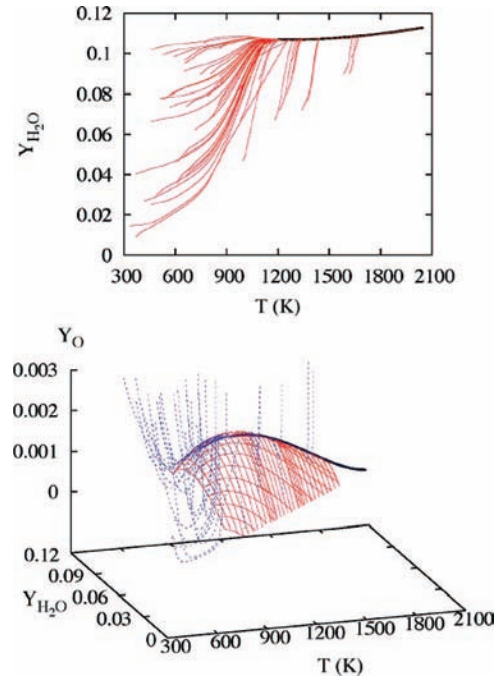

Figure 4. A subset of the trajectories generated for Figure 5 of ref 1 are plotted along with the one-dimensional manifold in the top panel and the two-dimensional manifold in the bottom panel. These plots show how the trajectories are attracted to the manifolds for the chemical-kinetic system.

III. Manifold Examples

A. A Chemical-Kinetic Example. The accuracy of the algorithms for one- and two-dimensional manifolds can be ascertained by observing how trajectories are attracted to the manifolds generated by them. A subset of the trajectories plotted in Figure 5 of ref 1 for the adiabatic, isobaric chemical-kinetic system is shown in the two panels of Figure 4. Once again, the chemical-kinetic system is fixed by a constant mixture enthalpy that matches the asymptotic enthalpy of the standard flame system with the elemental constants chosen in the same manner (eq 2.2 in ref 1).

The one-dimensional manifold is plotted in Figure 4 with a thick solid line along with the set of trajectories plotted with thinner, red lines. The top panel of Figure 4 demonstrates that the trajectories are attracted to the one-dimensional manifold, which starts at approximately $T = 1200$ K. The value of α_1 is 576.0 (eq 4.1a of ref 1), which is the ratio of the two least negative eigenvalues at the equilibrium point (all of the eigenvalues are negative at equilibrium). This value indicates that near equilibrium the manifold has strong attractive properties, with this highly attractive behavior evident away from equilibrium, down to approximately $T = 1200$ K, as trajectories appear to be strongly attracted to the manifold.

The bottom panel compares the same set of trajectories with the 2-D manifold generated as described above with three overlapping pieces spanning the temperature ranges: 850−1250, 1200−1500, and 1450−1800 K. This system has a value of $\alpha_2 = 30.3$ (eq 4.1b of ref 1), which is the ratio of the second and third least negative eigenvalue at equilibrium. Such a value of α_2 demonstrates that the manifold has strong attractive properties

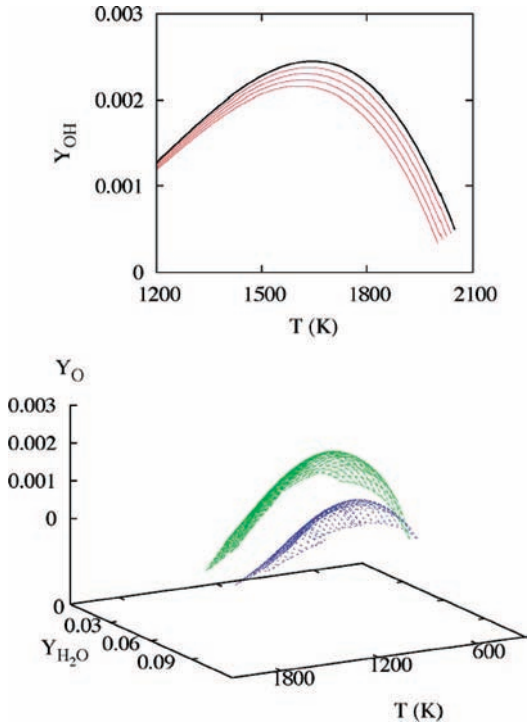

Figure 5. The top plot shows a series of five one-dimensional manifolds for five systems with the same elemental constants but with different enthalpies. The thick black line is for a system whose constant enthalpy is equal to the asymptotic enthalpy of the standard flame example. The bottom panel shows two-dimensional manifolds for systems with two different enthalpies.

near equilibrium, and the plot in the bottom panel makes it clear that the manifold is still attractive away from equilibrium.

The manifolds change as the chemical-kinetic system changes with the constants that are the mixture enthalpy and the elemental constants defined in eqs 2.2a−c of ref 1. The top panel of Figure 5 shows five 1-D manifolds for five systems. These systems all have the same elemental constants, which are chosen on the basis of the values at the saddlepoint of the standard flame system in Figure 2. The values of the enthalpy of the systems are chosen over the range of enthalpies along the one-dimensional flame manifold shown in Figure 2. The range is from approximately -7×10^8 ergs/g to the asymptotic value for the flame, -1.755×10^8 ergs/g (thick black line).

The two-dimensional manifolds also change as the chemical-kinetic systems change with their constants. Two two-dimensional manifolds are shown in the bottom panel of Figure 5 that nearly span the range of enthalpy of the two-dimensional manifold for the standard flame system (Figure 3). The upper green surface is at $H = 3 \times 10^9$ ergs/g, and the lower blue surface is at $H = -7 \times 10^8$ ergs/g. Once again, the other constants are the same as the asymptotic values for the standard flame system.

B. Flame Examples. Figure 6 demonstrates that the steady flame of ref 1 is first attracted to the two-dimensional manifold in the bottom panel (see Figure 3), then to the one-dimensional manifold in the top panel (see Figure 2). These plots demonstrate that the qualitative features demonstrated in several figures of ref 1 indeed correspond to motion on low-dimensional manifolds.

The analysis of the way trajectories are attracted to the manifolds is completed by examining a subset of the trajectories from Figure 17 of ref 1. The top panel of Figure 7 shows how the trajectories are attracted to the one-dimensional manifold

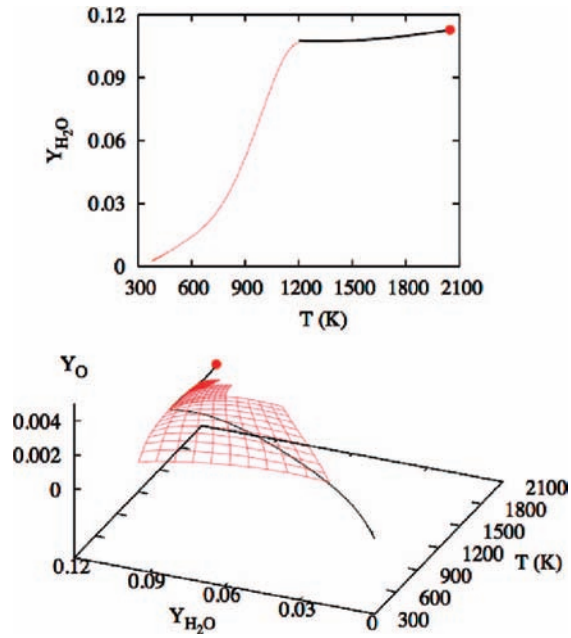

Figure 6. The one-dimensional manifold from Figure 2 is plotted in the top panel along with the steady flame from the standard flame system. In the bottom panel is plotted the same steady flame along with the two-dimensional manifold from Figure 3.

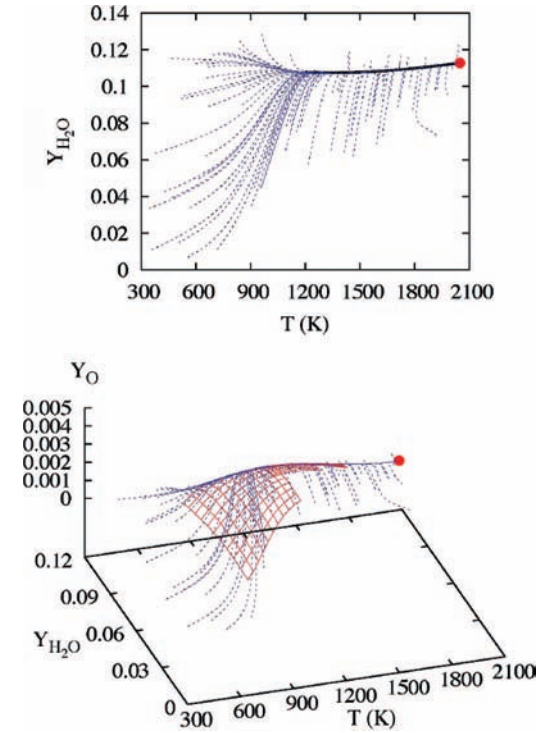

Figure 7. Trajectories of the standard flame system are compared to the one-dimensional manifold in the top panel (thick, dark line) and the two-dimensional manifold in the bottom panel.

of Figure 2, and the bottom panel of Figure 7 shows how the trajectories are attracted to the two-dimensional manifold of Figure 3.

C. Comparison with ILDMs. The manifolds generated above via Fraser's algorithm are now compared to ones generated with the ILDM algorithm of Maas and Pope,[6] which is a more approximate,[15,26] but common, algorithm. The ILDM algorithm is also generally a much faster algorithm, as is true for the calculations in this Article. The version of the ILDM

algorithm used here is a modification of the one in ref 23b, in that analytical eigenvector derivatives are not used here. In the rest of the Article, we refer to a manifold estimated from the algorithm described in ref 23b and below as an "ILDM". A manifold estimated from Fraser's algorithm is referred to as a "manifold", "iterated manifold", or "relaxed manifold". From past experience (see, for example, ref 15), Fraser's algorithm provides a very accurate estimate of the true manifold.

For the chemical-kinetic systems, one-dimensional ILDMs are estimated from the zeros of the following set of $n - 1$ equations:

$$R_{n1}(z_1)F_k(z_1) - R_{k1}(z_1)F_n(z_1) = 0,\ k = 1 \rightarrow n, k \neq m \quad (3.1)$$

where n is 6. As with the manifolds calculated with Fraser's algorithm in section II.B, the ILDM is defined along a progress variable (z_1) taken to be the temperature in this paper (eq 2.2a). All of the quantities in eq 3.1 have all of the other dependencies enumerated in section II.B, also. $R_{n1}(z_1)$ and $R_{k1}(z_1)$ refer to the nth and kth component of the right eigenvector whose eigenvalue is least negative along z_1. This eigenvalue is negative and real at equilibrium and generally is negative away from equilibrium (T less than the equilibrium temperature), but can become positive sufficiently far from equilibrium. The eigenvalue with lowest magnitude can also become part of a complex conjugate pair. At points where this happens, it is assumed there is not a good one-dimensional ILDM. Such a condition is common for general dynamical systems where trajectories spiral into equilibrium,[38] but for chemical-kinetic systems such behavior does not generally occur at equilibrium. Because we have taken a conervative approach to the convergence of the manifolds, as outlined above, we do not observe this behavior when generating one-dimensional manifolds. We do observe the behavior away from the one-dimensional manifolds, when two-dimensional manifolds are estimated.

For two-dimensional manifolds, the following $n - 2$ equations are solved for the chemical-kinetic system:

$$Q_{mp}F_k - Q_{kp}F_m + Q_{km}F_p = 0 \quad (3.2a)$$

with

$$Q_{mp} = R_{m1}(z_1, z_2)R_{p2}(z_1, z_2) - R_{p1}(z_1, z_2)R_{m2}(z_1, z_2) \quad (3.2b)$$

where R_{m2} and R_{p2} refer to the mth and pth components of the right eigenvector whose eigenvalue is second largest. As in section II.B, the ILDMs are characterized by two progress variables, z_1 and z_2, along their extent. The coordinate z_1 is once again taken as T for both the chemical-kinetic and the flame systems, and z_2 is once again Y_{H_2O} for chemical-kinetic systems and G_{H_2O} for flame systems.

The 1-D manifold of the chemical-kinetic system of Figure 4 is compared to the corresponding ILDM in the top panel of Figure 8, and the 2-D manifold is compared to the ILDM in the bottom panel. The 2-D manifold estimates are once again generated on overlapping grids. For the iterated manifolds, the grid is connected with solid lines. The ILDM grids are plotted on top of the grids for the iterated manifolds and are represented as a set of dots, which generally lie right on top of the iterated manifold grids. Therefore, these plots demonstrate that ILDMs are very good approximations to the more accurate iterated estimates for this chemical-kinetic system. The solid black line in the bottom panel repeats the iterated 1-D manifold from the top panel.

The calculation of ILDMs for flame systems requires extra care, as noted in ref 19. Generally, when ILDMs are estimated

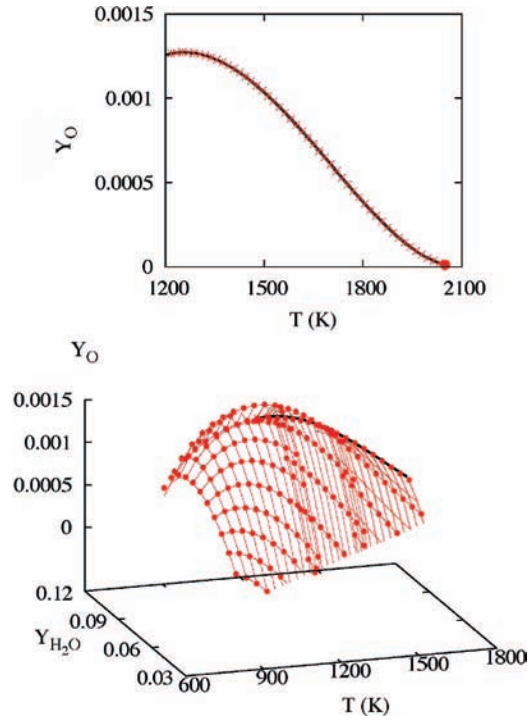

Figure 8. The 1-D ILDM is compared to a one-dimensional manifold generated via Fraser's algorithm for the chemical-kinetic system in the top panel, and the 2-D ILDM is compared to the 2-D manifold from Fraser's algorithm in the bottom panel. The iterated manifold is plotted with solid lines in both panels and the ILDM as a series of dots. Once again the 2-D manifold was generated in three pieces: 850−1250, 1200−1500, and 1450−1800 K.

for stable systems, positive eigenvalues are considered to lie on the ILDM, as was done above for the chemical-kinetic system. It is clear from the analysis in ref 1 that this is not a proper way to estimate manifolds within the ILDM formulation because the flame systems are dominated by a saddlepoint and the low-dimensional manifolds that are estimated are submanifolds of only the stable manifold of the system. So the following prescription is used, which is a modification of that in ref 19. Because the stable manifold at the saddlepoint is six-dimensional, it is assumed that the stable manifold is six-dimensional throughout the phase space. For a significant fraction of the phase space studied here, this is equivalent to ignoring the positive eigenvalues when calculating an ILDM, because in these regions there are exactly six negative eigenvalues. However, away from the fixed point, particularly for the 2-D manifolds, there are less than six negative eigenvalues, and then it is assumed that the eigenvectors associated with the other positive ones lie along the ILDM. These positive eigenvalues (some complex) arise when the smallest negative eigenvalues become positive; thus we view this prescription as consistent.

Figure 9 compares the low-dimensional manifolds for the flame with the ILDMs. The top panel shows a comparison between the 1-D manifold estimates, with the dots showing the ILDM. As in the chemical-kinetic case, there is excellent agreement between the ILDM and the iterated estimate. The bottom two panels show comparisons between the two-dimensional ILDMs and the relaxed manifolds. The lines show constant temperature isoclines of both surfaces. The iterated manifolds are drawn as solid lines, and the ILDM estimates are drawn as dashed lines. The middle panel shows isoclines for the temperature range 800−1250 K, and the bottom panel shows the range 1200−1500 K, the two pieces of the manifold

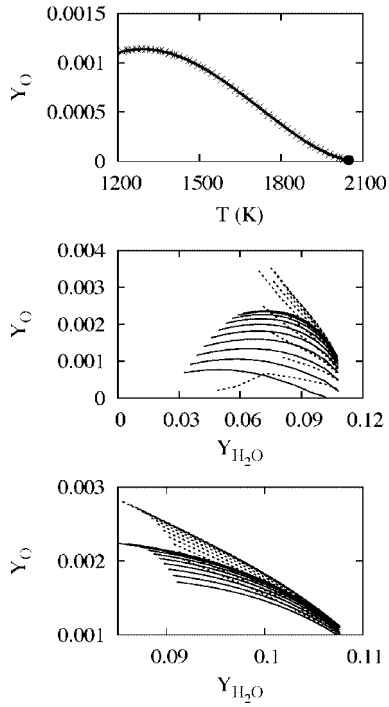

Figure 9. The top panel compares the 1-D manifold for the ILDM (dots) with the iterated version (solid line). The bottom two panels compare isoclines of the 2-D manifolds. The solid lines show the iterated manifold, and the dashed lines show the ILDM. The middle panel shows the low temperature piece (800−1200 K) and the bottom the middle piece (1250−1500 K) from the manifold of Figure 3.

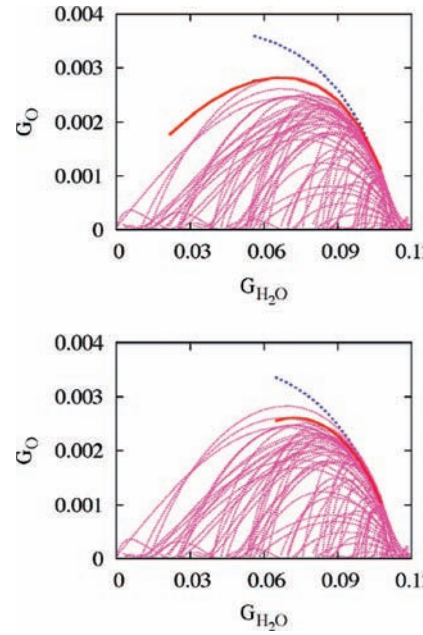

Figure 10. Trajectories (dotted lines) are compared to isoclines of the iterated surface (solid red lines) and ILDM (dashed lines) in the two plots. The top plot shows the $T = 1250$ K isocline, and the bottom panel shows the $T = 1440$ K isocline.

presented in Figure 3 and Figure 7. In both sets of panels, the ILDMs differ significantly from the more accurate iterated manifold. At the lowest temperatures in the middle panel, the ILDM conditions are not always met, and the ILDM estimates have shorter isoclines than the iterated manifold. The bottom two panels demonstrate that, unlike for the chemical-kinetic system, the flame system has a considerable difference between the iterated manifold and the ILDM.

The relative accuracy of the ILDMs as compared to the iterated manifolds can be gauged by investigating the approach of trajectories to them. The comparison is most straightforward using the mass flux fractions rather than the mass fractions. The top panel of Figure 10 shows such a projection for the $T = 1250$ K isoclines of the iterated manifold (solid lines) and the ILDM (dashed lines) along with trajectories from Figure 7. The bottom panel repeats the trajectories along with the $T = 1440$ K isoclines for the iterated manifold (solid line) and ILDM estimates (dashed line). These panels demonstrate that the iterated 2-D manifold is a much better representation of the asymptotic behavior of trajectories than the 2-D manifold estimated from the ILDM algorithm.

IV. Relationship between Chemical Kinetics and Steady-State Flame Dynamics

In this section, comparisons are made between the manifolds of the flame systems and the manifolds of the chemical-kinetic systems. Because ILDMs may not be accurate estimates of two-dimensional manifolds for the flame systems (for example, Figures 9 and 10), the initial set of comparisons of the manifolds in this section are made only with the algorithms described in section II.B. We expect that the manifolds generated with this algorithm are essentially exact for both the flame systems and the chemical-kinetic systems, allowing for the best possible comparison between the manifolds of the two types of systems. However, it proved interesting to compare the two-dimensional flame manifolds generated with the more accurate algorithm to chemical-kinetic manifolds generated from the ILDM algorithm, and this is done in the latter plots in this section (Figures 15–17).

A. One-Dimensional Manifold Comparisons. To make comparisons between the chemical-kinetic manifolds and the flame manifold, the following is done. The elemental chemical-kinetic constants (eq 2.2 in ref 1) and mixture enthalpy are calculated along the 50 points that are used to define the flame manifold in Figure 2. For each of these points, the constants define a different adiabatic, isobaric chemical-kinetic system. The equilibrium point of each of these systems is found, and then the manifold method of section II.B is used to calculate a one-dimensional manifold for the chemical-kinetic system. The series of dots in the top panel of Figure 11 show the results of this calculation plotted on top of the one-dimensional flame manifold for the standard flame system. The dots in the top panel are a composite of a series of one-dimensional manifolds for a set of chemical-kinetic systems.

The bottom panel of Figure 11 shows an expanded view of the information from the top panel with an additional series of curves. These curves, plotted as dashed lines, show a small portion of the chemical-kinetic manifolds generated at every fifth point along the flame manifold. This information, along with the top plot, indicates that the composite of the chemical-kinetic manifolds is an excellent representation of the one-dimensional flame manifold, despite the difference in the two types of manifolds, as comparison between the solid line and the dashed lines of the bottom panel demonstrates.

B. Two-Dimensional Manifold Comparisons. Comparisons between the two-dimensional manifold of Figure 3 and chemical-kinetic composites are made in Figure 12. The three panels show the three pieces of the manifold plotted originally in Figure 3 in order from low temperature (top) to high temperature (bottom). The solid lines show the isoclines of the flame manifold, and the dashed curves show the chemical-kinetic composites. The isoclines are similar, but differences arise for

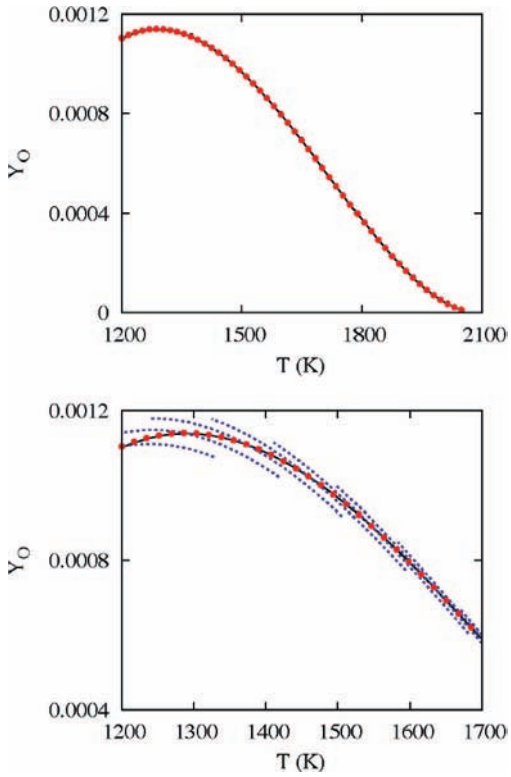

Figure 11. The flame manifold is compared to a composite of the chemical-kinetic manifolds. The top panel compares the flame manifold (solid line) with the chemical-kinetic composites (dots). An expanded view is shown in the bottom panel along with portions of the chemical-kinetic manifolds used to generate the composite.

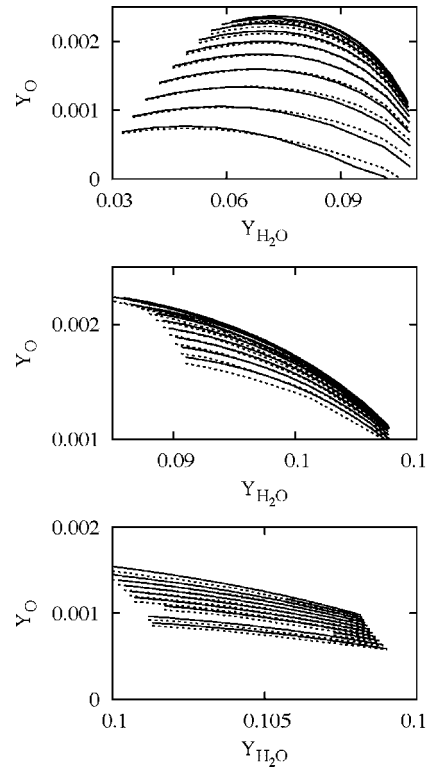

Figure 12. Comparisons are made between the chemical-kinetic composites and the flame manifold of Figure 3. These panels show isoclines for the low temperature (top), mid temperature (middle), and high temperature portions of the manifold of Figure 3. The solid lines show isoclines of the flame manifold, and the dashed lines show chemical-kinetic composites. The ranges of the manifold sections are described in section II.C and are the same as in Figure 3: 800−1250 K (top), 1200−1500 K (middle), and 1450−1700 K (bottom).

the Y_O/Y_{H_2O} projection as the one-dimensional manifold is approached for higher values of Y_{H_2O}.

Additional information concerning the comparison is presented in Figure 13, which shows all of the other projections of Y_k/Y_{H_2O} for the low-temperature isoclines. Once again, the solid lines show the flame isoclines, and the dashed lines show the chemical-kinetic composites. These projections demonstrate that the Y_O/Y_{H_2O} projection in Figure 12 has the poorest agreement between the chemical-kinetic composites and the flame manifold.

The comparison of the composite 2-D chemical-kinetic manifold and the 2-D flame manifold is completed in Figure 14, which shows how a single composite temperature isocline is formed from 2-D chemical-kinetic manifolds. The top left panel compares the flame manifold along the $T = 890$ K isocline of the 2-D manifold. It is shown projected in two ways in the panel. The upper curve plotted as a solid line shows a Y_O/Y_{H_2O} projection, and the bottom curve shows a Y_{OH}/Y_{H_2O} projection. The dotted line on top with dots shows the composite chemical-kinetic isocline, and the dashed line in the lower part of the panel shows the chemical-kinetic composite. The chemical-kinetic and flame projections are very close. The Y_O/Y_{H_2O} projections differ by a small amount at the largest values of Y_{H_2O}, and the Y_{OH}/Y_{H_2O} projections lie on top of each other. This panel re-emphasizes what Figure 12 and Figure 13 have shown previously.

The rest of the panels in Figure 14 compare the surface for the 2-D chemical-kinetic manifolds (solid lines) used to generate the composite surface with the 2-D flame manifold (dotted lines). These panels correspond to points 2, 4, 6, 8, and 10 (the dots, left to right) in the top left panel. The chemical-kinetic surfaces are generated at a set of chemical-kinetic constants fixed at the point on the flame manifold where the comparison is made. The point of comparison is plotted as a large dot on each flame manifold and as an "x" on each chemical-kinetic manifold. While not as accurate as the analogous one-dimensional case in Figure 11, the chemical-kinetic composites are much more accurate than what may appear by comparing the full surfaces in Figure 14, which can look quite different away from the point of comparison.

Two-dimensional flame manifolds generated from the ILDM algorithm do not agree with the more accurate iterated manifolds, as demonstrated in Figure 9. However, Figure 8 in section III.C demonstrated that for adiabatic, isobaric chemical kinetics, two-dimensional manifolds generated with the ILDM algorithm do agree with the more accurate iterated manifolds generated for the same chemical-kinetic system. Because of this agreement, we thought it would be interesting to compare chemical-kinetic composites generated from ILDMs with the accurate iterated flame manifolds, as was done in Figures 12–14 where comparisons were made between flame manifolds and chemical-kinetic manifolds both generated from the more accurate iteration algorithm. The comparisons between the iterated flame manifolds and the chemical-kinetic composites generated from the ILDM algorithm are presented in Figure 15. Figure 15 repeats the two-dimensional iterated manifold from Figure 3 in the three pieces it was generated and compares the three pieces to the appropriate chemical-kinetic ILDM composites. The two-dimensional flame manifold is plotted with dashed lines, and the chemical-kinetic ILDM-estimated composite manifolds are plotted as a series of dots. Once again, these points are generated at the values of the chemical-kinetic constants and enthalpy that

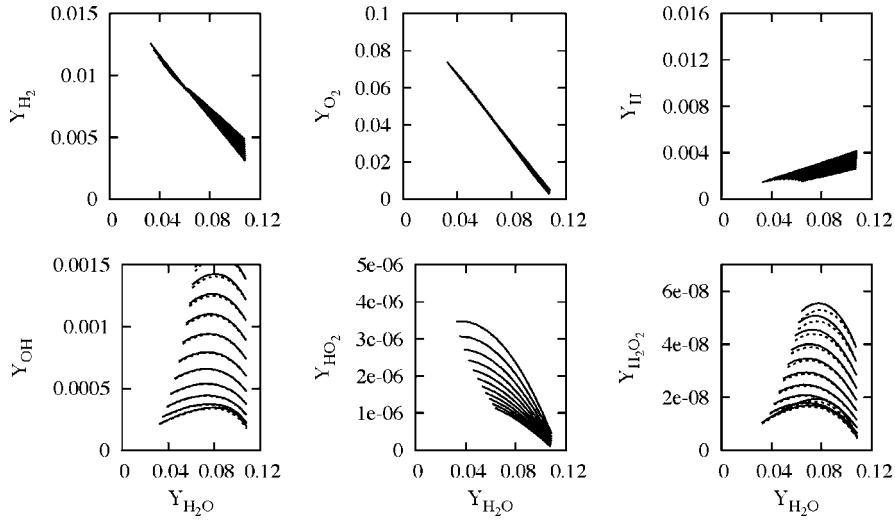

Figure 13. These plots are different projections of the top panel of Figure 12.

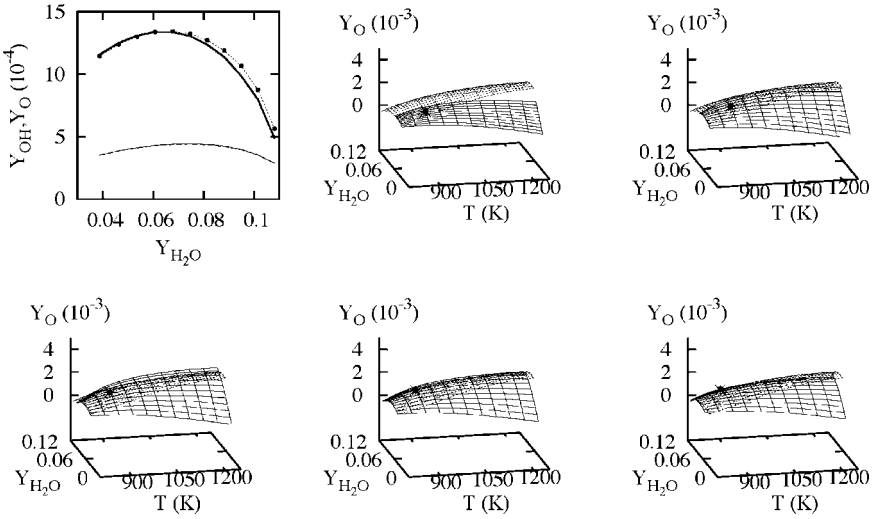

Figure 14. These plots demonstrate how the composite isoclines of Figure 12 are generated. The top left panel repeats two projections of the isocline, and the surfaces presented in the rest of the panels show the chemical-kinetic manifold generated at that point and repeats the flame manifold as a surface plotted with dotted lines. The relevant point along the isocline is shown as a dot for the chemical-kinetic manifold and an "×" for the flame manifold.

correspond to the equivalent point on the flame manifold. Generally, the comparisons are similar to what is observed in Figure 12.

The relatively good accuracy of the ILDM for the chemical-kinetic manifolds allows a more detailed comparison that bolsters the view given in Figure 12. Figure 16a and b shows all of the temperature isoclines of the two-dimensional flame manifold from the top and middle panels of Figure 12. These are plotted as solid lines along with dotted lines showing the composite chemical-kinetic manifolds. The flame manifold and the chemical-kinetic composites are iterated manifolds. These are compared to the ILDM estimates of the composite chemical-kinetic manifolds plotted as a dotted line. The curves in Figure 16a, especially those in the bottom row, give additional support for the difference between the chemical-kinetic composites and the two-dimensional flame manifolds, because the iterated chemical-kinetic manifold composites and the equivalent ILDM composites lie on top of each other and are noticeably different than the isoclines for the two-dimensional flame manifold.

Previous results in section III.C demonstrated that the ILDM approximation was very accurate for the chemical-kinetic system for both one- and two-dimensional manifolds and for one-dimensional manifolds of the flame system. However, the ILDM approximation was inaccurate for the two-dimensional manifolds of the flame system. A comparison of all of these results is made for a two-dimensional manifold in Figure 17.

Two isoclines are plotted as solid lines in Figure 17. The top panel shows an isocline at $T = 890$ K, and the bottom panel shows an isocline at $T = 1380$ K. The lines plotted with dashes are the ILDM for the flame and are very different from the isocline of the iterated surface. This inaccuracy was made clear in Figure 9 above. The two other curves on both plots are the composite chemical-kinetic isocline plotted as a dotted line as generated for Figures 13 and 14. The curves plotted with thicker dashes are composite isoclines generated within the ILDM approximation. Figure 17 demonstrates that the worst approximation to the two-dimensional manifold is generally an ILDM approximation of the flame manifold and that this is worse than a composite ILDM generated from chemical-kinetic systems. This result disagrees with ref 19, which found that flame ILDM manifolds were better for the system they studied. It is not clear why this is true. Further investigation of this discrepancy would be interesting.

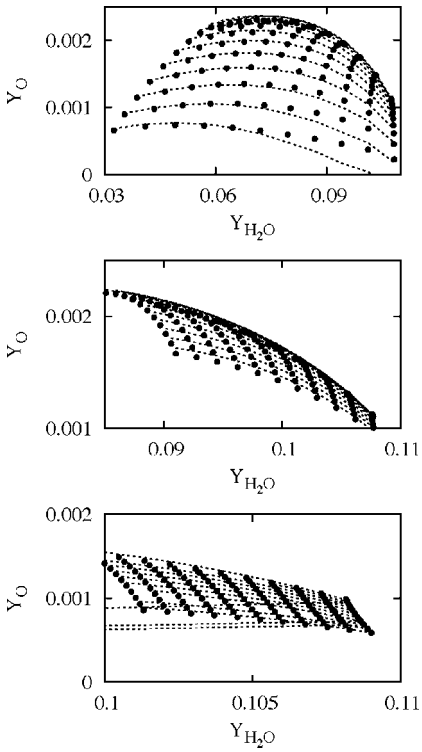

Figure 15. A comparison is made here between the temperature isoclines of the two-dimensional flame manifolds and the chemical-kinetic composites estimated from the chemical-kinetic ILDMs. The three panels repeat the temperature ranges of the manifold in Figure 3, from top to bottom: 800−1250 K, 1200−1500 K (middle), and 1450−1700 K (bottom).

V. Trends

Figures 12 and 13 of ref 1 presented results for a range of systems that changed with stoichiometry and enthalpy. In this section, many of the calculations in the present Article are applied for nine systems chosen over the range of parameters presented in those figures. This range is narrower in stoichiometry than the systems in Figures 12 and 13 in ref 1, but has nearly the same range of enthalpy.

Table 1 summarizes the nine systems. The first column lists a stoichiometric factor defined implicitly in eq 4.2 of ref 1, which in turn defines the set of constants described in eq 3.2 of ref 1. These constants, along with the asymptotic enthalpy, define the flame systems, with the second column giving the asymptotic enthalpy for the nine flame systems. Table 1 also defines a set of nine chemical-kinetic systems. These systems have constant enthalpy, and this is taken to be the asymptotic enthalpy of the flames listed in the second column. The additional constants for the chemical-kinetic systems are listed in columns 3 and 4 and defined in eq 2.2 of ref 1. These constants are the asymptotic values of these quantities for the flame systems.

Figures 12 and 13 of ref 1 laid out the way in which the attractivity of manifolds changed with stoichiometry and enthalpy based on the ratio of the negative eigenvalues of the Jacobian at the saddlepoint, and the results presented in Table 1 are consistent with the results of Figures 12 and 13. The first column groups the systems into lean ($\chi_s = 0.5$), stoichiometric ($\chi_s = 1.0$), and rich ($\chi_s = 1.5$). For each of these mixtures, a low enthalpy (0.0 ergs/g), medium enthalpy (3×10^9 ergs/g), and high enthalpy case (6×10^9 ergs/g) is considered. The final four columns list the attractivity of the one- and two-dimensional manifolds at the fixed points of the chemical-kinetic (columns 5 and 6) and flame (columns 7 and 8) systems. These numbers demonstrate that all systems have highly attractive one-dimensional manifolds near the equilibrium/saddlepoint, but many of them do not have very attractive two-dimensional manifolds, suggesting once again that the ILDM approximation may not be accurate for these cases, based on past experience.[15,26]

The subsequent subsections of this Article examine results for these nine systems.

A. Low-Dimensional Manifolds for the Flame Systems. In Figure 18, the calculations from the top panel of Figure 2 are repeated for the nine systems of Table 1. Manifolds were generated from a set of calculations from the saddlepoint to a minimum temperature where convergence could be achieved between 1200 and 1000 K. However, more information is presented in Figure 18 than in Figure 2, because plots include all of the manifolds generated with end points between 1600 K and the minimum temperature where convergence can be achieved, between 1200 and 1000 K at 20 K increments, whereas Figure 2 used only those at 100 K increments. Most of the manifolds in Figure 18 are plotted with thin solid lines, but 6 of them have special line types. The manifold out to 1600 K is plotted with large dots, the segment out to 1500 K as small dots, the segment out to 1400 K as a thick dashed line, the segment to 1300 K is a thick solid line, the one to 1200 K is a dashed−dotted line, the one to 1100 K is a short dashed line, and the final one to 1000 K is a dotted line. It is possible to converge the manifolds of lean flames in the top row out to only about 1200 K, while the stoichiometric flames in the middle row could be converged to approximately 1120 K (the highest enthalpy case) down to below 1100 K for the lower two enthalpy cases. In the bottom row, the lowest and highest enthalpy cases could be converged to 1000 K and the middle enthalpy case to below 1100 K.

Although the algorithm converges below 1200 K for many of the cases in Figure 18, the plots in Figure 18 indicate that most of these cases do not show strong convergence below 1200 K, because manifolds generated out to lower temperatures do not lie on top of the ones generated out to higher temperatures. This is most obvious in the high enthalpy case for the rich flame in the bottom right, where the manifold is perhaps not even converged to 1200 K. It is results such as these that led us to make the estimate, stated in section II, that one-dimensional submanifolds of the stable manifold were attractive from the saddlepoint down to about 1200 K, and all of the comparisons made in previous sections of the Article involved a one-dimensional manifold that extended from 1200 K to a saddlepoint temperature of 2050 K.

The analysis of the one-dimensional manifolds is completed in Figure 19, with a set of calculations that are the same as those of the middle panel of Figure 2. The manifolds generated in Figure 18 via 20 K extensions of the one-dimensional manifolds are compared to manifolds generated directly from the relaxation of a linear segment from the saddlepoint out to 1200 K. The manifolds out to 1200 K from Figure 18 are plotted as solid lines in Figure 19 and compared to the direct method drawn as a series of dots. Figure 19 demonstrates that the direct calculation is as accurate as the incremental method.

The analysis of the two-dimensional manifolds for the nine systems is presented in Figure 20, where calculations of two-dimensional manifolds are presented. These are calculated in the manner of section II.C as shown for the standard flame system in Figure 3. Once again, these manifolds are generated in three overlapping pieces. It was possible to converge the lean flames in the top row out to 850 K. The stoichiometric flame systems in the middle row and the rich flame systems in the

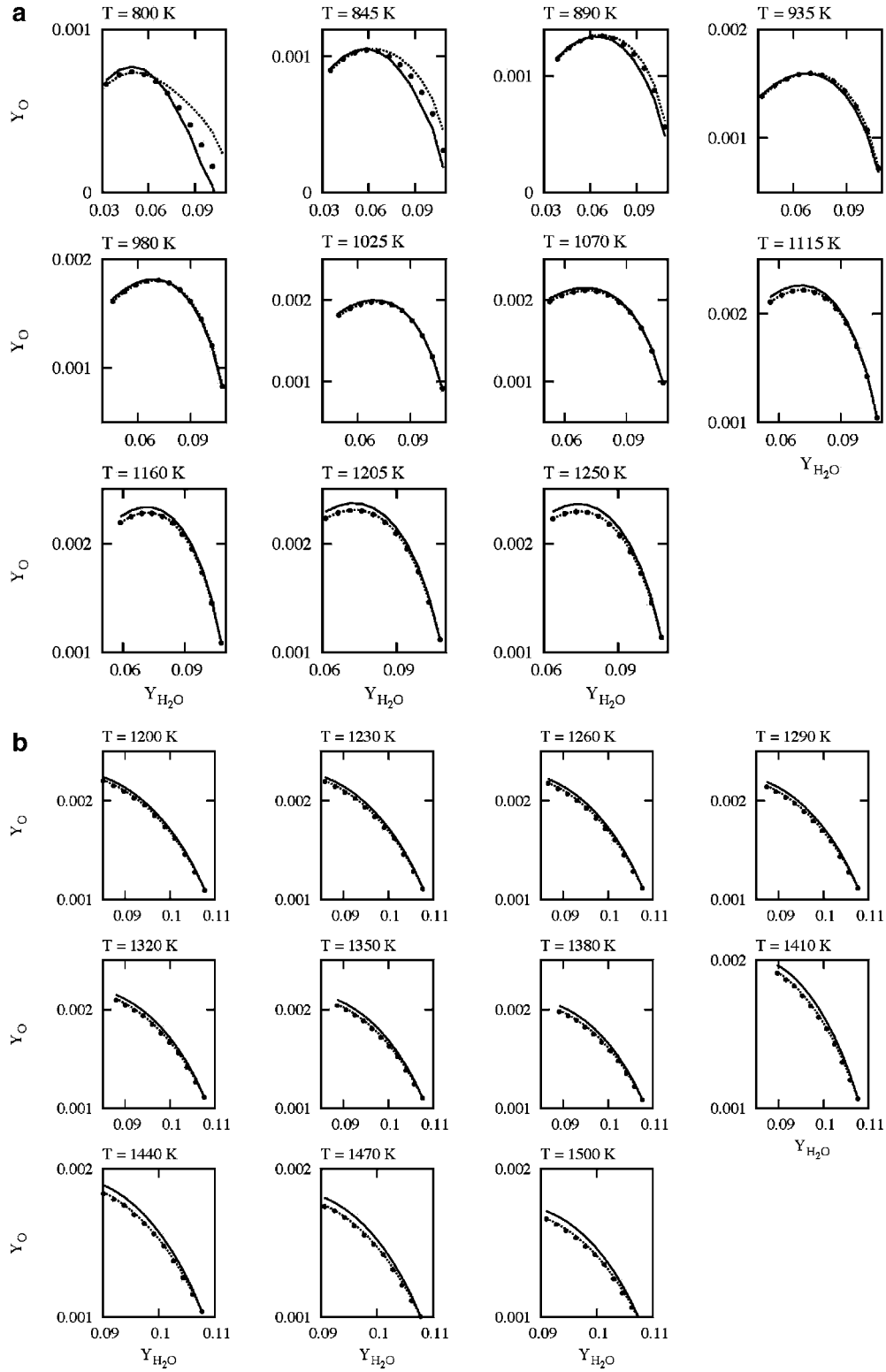

Figure 16. (a) A comparison of the isoclines for the low-temperature portion of the two-dimensional manifold from Figure 12 (solid line) as compared to the iterated composite chemical-kinetic isocline (dots) and the ILDM version of this curve (dotted line). (b) This is a continuation of (a), showing isoclines for the middle temperature range of 1200−1500 K.

bottom row were converged out to 800 K, and the high temperature pieces are converged to 1800 K. So the full range of the manifolds for all three pieces is 850−1800 K for the lean flames in the top row and 800−1800 K for the stoichiometric and rich flames in the bottom two rows. The lowest enthalpy lean flame had a two-dimensional manifold that was very narrow for the highest temperature portion and is not included in the manifold on the top left of Figure 20.

Figure 20, like Figure 3 in section II, includes several trajectories started on the two-dimensional manifolds. These trajectories stay on the calculated manifold as they move to the saddlepoint, demonstrating that the two-dimensional manifolds are invariant surfaces for all of the flame systems.

B. Comparison to ILDMs. ***1. Chemical Kinetics.*** Table 1 indicates that the one-dimensional manifolds for the chemical-kinetic systems are strongly attractive near equilibrium. Gener-

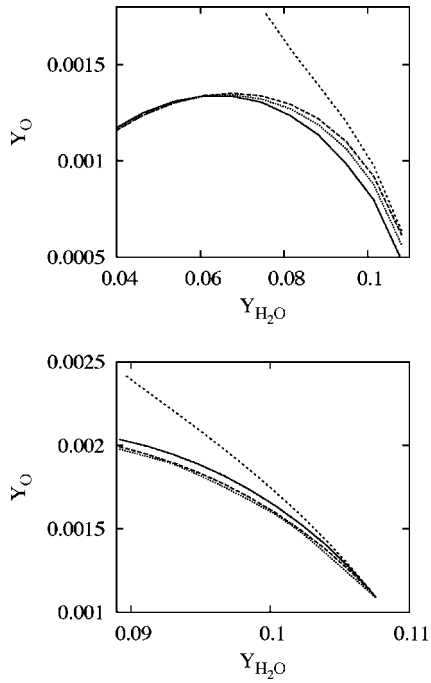

Figure 17. A comparison is made between isoclines for the two-dimensional manifold of Figure 12. The solid lines show isoclines for the accurate iterated two-dimensional flame manifold, and the dashed line shows the inaccurate ILDM estimate. The dotted lines and the thicker dashes show the iterated chemical-kinetic composites and their ILDM approximates, which are very close and better approximations to the accurate, iterated flame manifold than is the ILDM estimate. The top panel shows the $T = 890$ K isocline, and the bottom panel shows the $T = 1380$ K isocline.

TABLE 1: Summary of Fixed Point Properties of Nine Systems

χ_s[a]	$\bar{h}_\infty$[b]	c_O[c]	c_{Ar}[c]	α_1[d]	α_2[d]	α_{1f}[d]	α_{2f}[d]
0.5	0.0	0.012	0.80	824.6	3.59	200.4	2.52
0.5	3×10^9	0.012	0.80	947.8	2.53	150.7	2.13
0.5	6×10^9	0.012	0.80	953.6	2.22	120.4	1.97
1.0	0.0	0.0083	0.85	532.4	8.42	132.4	2.89
1.0	3×10^9	0.0083	0.85	560.9	6.43	109.6	2.43
1.0	6×10^9	0.0083	0.85	594.7	5.37	98.2	2.17
1.5	0.0	0.00645	0.88	552.0	27.8	319.4	7.59
1.5	3×10^9	0.00645	0.88	608.7	16.4	219.6	3.61
1.5	6×10^9	0.00645	0.88	636.8	9.4	164.9	2.57

[a] Stoichiometry defined in eq 4.2 in ref 1. [b] Asymptotic mixture enthalpy of the flame and constant enthalpy of the adiabatic, isobaric chemical-kinetic system. In units of ergs/g. [c] The constants of the saddlepoint, where chemical-kinetic and flame constants are equal. See, for example, eqs 4.2f and 4.2g in ref 1. [d] Ratios defined in eqs 4.1a and 4.1b of ref 1. The subscript "f" refers to values for the flame system.

ally, for one-dimensional manifolds, there is good agreement between the ILDM estimates[6] and accurate manifolds when the manifolds are very attractive.[15,26] This was the situation for the standard flame example in the top panel of Figure 8, and an analysis of the one-dimensional manifolds indicates it is true for the nine systems of Table 1. There is generally near perfect agreement between the iterated manifolds and the ILDMs.

A comparison of the iterated two-dimensional manifolds with their ILDM counterparts for the chemical-kinetic systems has also been made, as defined above. The stoichiometric and rich cases have the same excellent agreement as the one-dimensional manifolds and the two-dimensional manifold in the bottom panel of Figure 8. However, there are some small discrepancies in the lean cases near $T = 1000$ K and the highest values of Y_{H_2O}. These systems have the least attractive manifolds and so are most likely to have inaccurate ILDM estimates.[15,26]

2. Flames. The top panel of Figure 9 demonstrated that there was good agreement between the ILDM and the more accurate relaxed one-dimensional flame manifold. This agreement extends to the flame systems in Table 1 as Figure 21 demonstrates. Based on the eigenvalue ratios in Table 1, this result is not unexpected. However, Figure 18 indicated that some of the manifolds appear to be relatively unattractive near $T = 1200$ K, particularly the rich, high enthalpy case in the bottom right of Figure 18. This case still has good agreement between the ILDM and the more accurate manifold as demonstrated on the bottom right of Figure 21.

The good agreement between the relaxed manifolds and the ILDM estimates for one-dimensional manifolds is not evident for the two-dimensional manifolds, something previously demonstrated for the standard flame system in Figure 9. The low-temperature pieces (Figure 20) shown in Figure 22a have particularly strong differences. Temperature isoclines of the relaxed manifolds are plotted as solid lines in Figure 22a, and the dots show the ILDM estimates, which often do not extend across the full isocline, because the ILDM criterion of eq 3.2a is not satisfied. This is most evident at the lower values of Y_{H_2O}, which are the furthest away from the one-dimensional manifold.

The comparison of the ILDMs with the iterated manifold is continued in Figure 22b for the intermediate temperature portions of the manifolds of Figure 20. In this temperature range, one of the systems exhibits reasonably good agreement between the ILDM and the relaxed manifold, the lean, low-enthalpy case in the top left of Figure 22b.

Figure 22c continues the trend of Figure 22b. There is now better agreement between the two types of manifolds, with very good agreement for the lowest enthalpy case of the stoichiometric and rich flame systems in the left column and the intermediate enthalpy case of the lean flame at the top of the middle column in Figure 22c. The agreement, or lack of agreement, shown in Figure 22a−c tracks reasonably well with the eigenvalue ratios shown in the right-hand column of Table 1 at the saddlepoint. There is not completely a one-to-one correspondence, although these cases are sufficiently far from the saddlepoint that discrepancies are not surprising. A visual inspection of the way trajectories approach the manifold in the various temperature regions for all of the systems suggests that these discrepancies are consistent with the dynamical behavior of the systems. That is, the more attractive that the manifold appears to be, the better is the agreement between the more accurate manifold estimates and the ILDM estimates.

C. Flame Manifolds versus Chemical-Kinetic Manifolds. Comparisons are now made between flame manifolds and chemical-kinetic composites for the nine flame and chemical-kinetic systems of Table 1. All comparisons are made between manifolds generated with the iteration-relaxation algorithm of section II.B.

1. One-Dimensional Manifolds. The chemical-kinetic one-dimensional composite manifolds are generally in very good agreement with the one-dimensional flame manifolds for the systems of Table 1 as Figure 23 demonstrates. These results are consistent with results for the standard flame system presented in Figure 11 of section IV.A.

Figure 23 shows the flame manifolds as solid lines and the chemical-kinetic composite manifolds as a series of dots. A piece of each chemical-kinetic manifold is shown as a dotted line in Figure 23 for every fifth point of the composite manifold. Figure

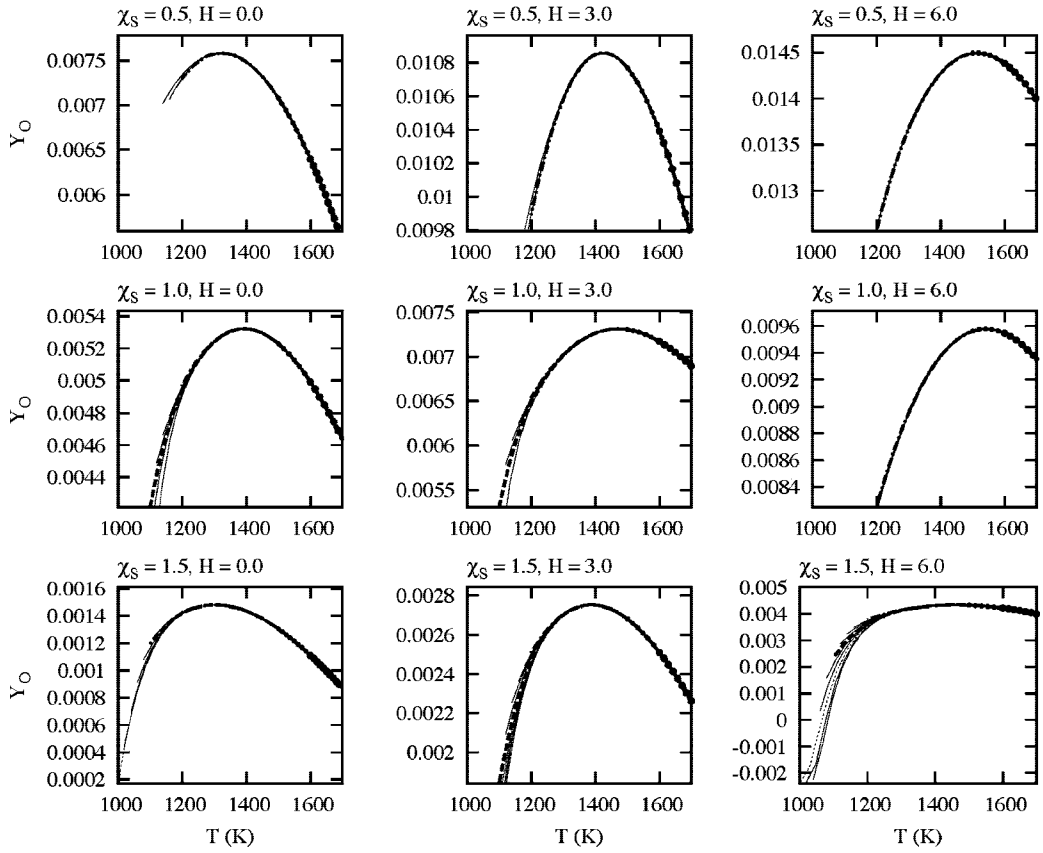

Figure 18. Calculations from the top panel of Figure 2 are repeated in these plots for the nine systems of Table 1. The various lines and symbols have the same meaning as they did in Figure 2, as described in the text of this section. *H* refers to the asymptotic mixture enthalpy in 10^9 ergs/g, as illustrated in column 2 of Table 1.

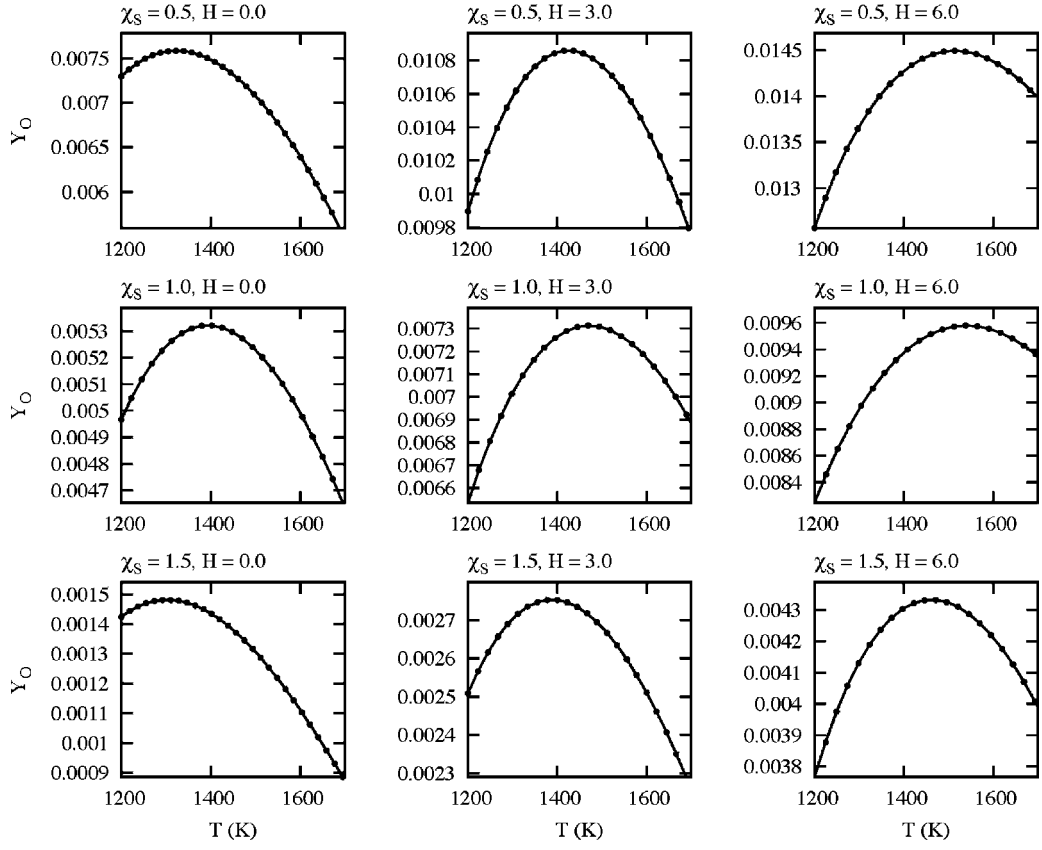

Figure 19. These plots repeat the calculation of the middle panel of Figure 2 for the nine systems of Table 1. Once again, the solid line plots the one-dimensional manifold as calculated in increments, as in Figure 18, with the direct calculation from a linear segment out to 1200 K. These plots show excellent agreement between these two methods.

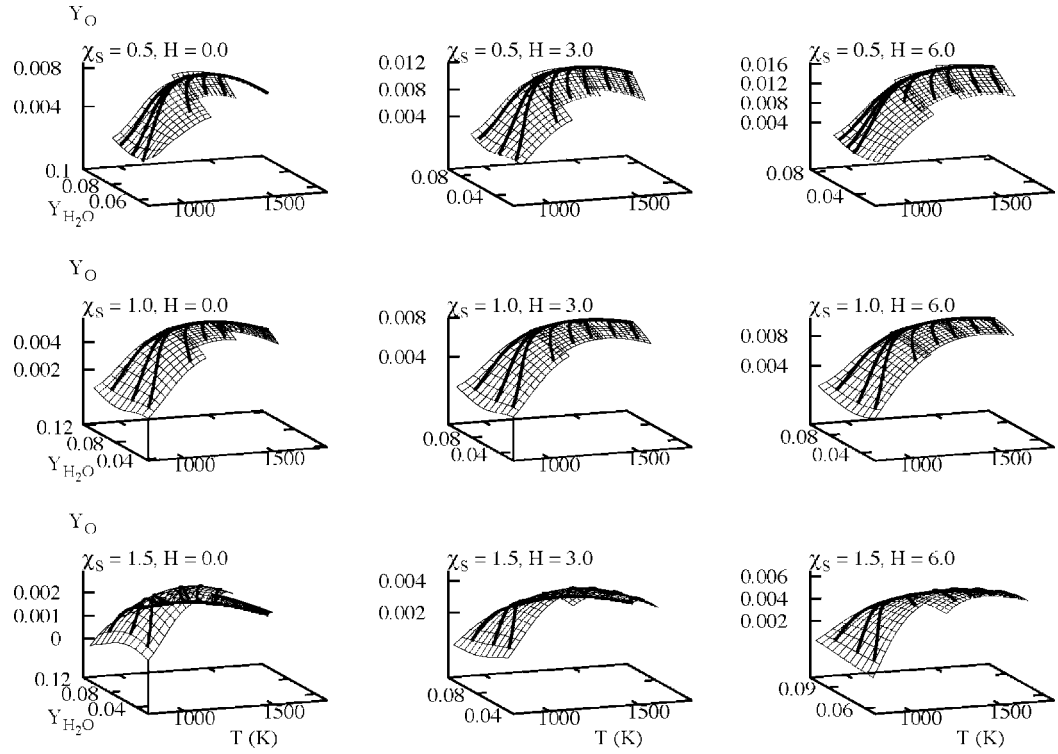

Figure 20. A series of two-dimensional manifolds for the nine systems of Table 1 are presented along with trajectories. The calculations reported here are the same as those in Figure 3. All manifolds were generated in three portions as before. The plot in the top left does not include the highest temperature portion, which is very narrow.

23 indicates that the composite manifolds are in excellent agreement with the flame manifolds, with only small differences near $T = 1200$ K for all of the cases plotted. These plots show Y_O/T projections, and the values of Y_O are generally the least accurate in relative terms except for the very low trace species such as H_2O_2 and HO_2.

2. Two-Dimensional Manifolds. Two-dimensional manifolds are harder to approximate than one-dimensional manifolds with the chemical-kinetic composites, as previously indicated in Figures 12–14. Isoclines for the lowest temperature portions are shown in Figure 24a. The isoclines of the flame manifolds are drawn with solid lines, and the chemical-kinetic composites

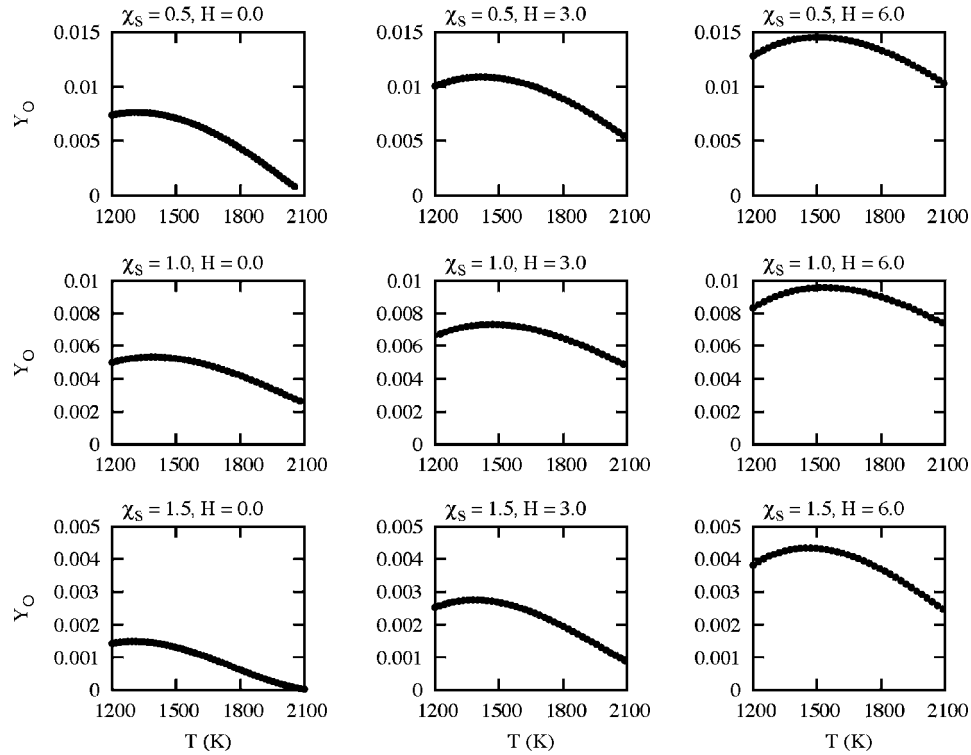

Figure 21. A set of comparisons between the one-dimensional flame manifolds for the nine systems of Table 1 (solid lines) and the ILDM estimates for the same systems (dots).

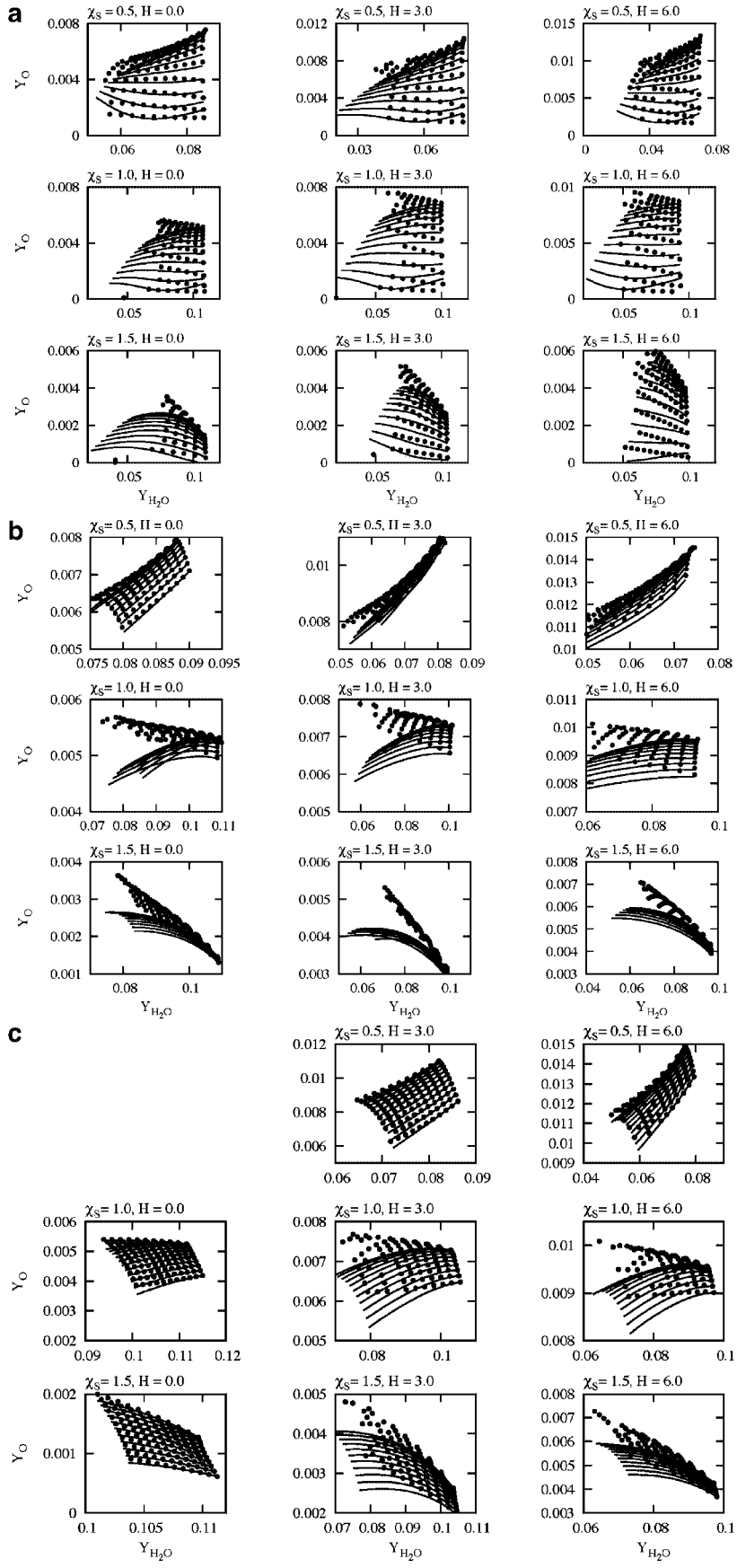

Figure 22. (a) A series of comparisons of the isoclines of the two-dimensional flame manifolds (solid lines) and the ILDM estimates for the nine systems of Table 1 for the low-temperature portions of the two-dimensional manifolds of the flame systems of Figure 20 in the same order as they appear there. (b) These plots repeat the calculations of (a) for the middle temperature portions of the 2-D manifolds of Figure 20. (c) The high-temperature versions of the comparisons of (a) and (b) are shown in a series of plots for the manifolds of Figure 20.

are drawn with dashed lines. Agreement is best for the rich flames in the bottom row of Figure 24a, but is poor for the lean cases in the top row. For the stoichiometric systems in the middle row, the chemical-kinetic isoclines differ somewhat at low values of Y_{H_2O}, but agree very well at high values of Y_{H_2O}, as the two-dimensional manifold approaches the one-dimensional manifold.

The intermediate temperature portions of the two-dimensional manifolds presented in Figure 24b show worse agreement between the chemical-kinetic composite manifolds and the flame manifolds than do the lower temperature ones over most of the extent of the isoclines. However, these cases show very good agreement along the isoclines near the one-dimensional manifolds, as expected from Figure 23. The one-dimensional manifolds are at the highest values of Y_{H_2O} shown in Figure 24b. Unlike the lower temperature pieces of the two-dimensional manifolds shown in Figure 24a, the one-dimensional manifolds, which extend down to 1200 K, encompass the full temperature range of Figure 24b.

The highest temperature portions of the isoclines for the flame manifolds and the chemical-kinetic composites are shown in Figure 24c. These portions of the manifolds extend over a relatively small portion of phase space, as indicated by the ranges on the axes. The manifolds are generally in better agreement than the intermediate temperature cases of Figure 24b. However, the two highest enthalpy cases of the stoichiometric flame systems in the middle row of Figure 24b show considerable disagreement between the chemical-kinetic composites and the flame manifolds except near the one-dimensional manifolds, which are at the highest values of Y_{H_2O} pictured and where the system is most attractive (it takes on characteristics of the relatively strong attractive nature of the one-dimensional manifold).

A better view of selected isoclines and the surfaces that were used to generate them are presented in a series of plots in Figures 25–27. These figures are analogous to Figure 14 that was generated for the standard flame system. Figures 25–27 also provide more expanded views of the comparisons of the isoclines in the upper leftmost panels.

The top left panel of Figure 25 shows two projections of a $T = 1050$ K isocline for the lowest enthalpy, lean system. The thicker solid line and the dotted line with the large dots on it show Y_{H_2O}/Y_O projections, and the dashed line and thinner solid lines show Y_{H_2O}/Y_{OH} projections. The flame isoclines are plotted with solid lines, and the others show the chemical-kinetic composites. Because T is below 1200 K, there is no converged one-dimensional manifold at this temperature.

The rest of the panels in Figure 25 show the surfaces used to generate the composite isoclines plotted as solid lines, and each of the panels shows the flame manifold as a grid made up of dotted lines. The points along the isocline where the composite was made are explicitly shown in each panel. The point along the flame manifold is shown as a solid dot, and the chemical-kinetic point is shown as an "×".

The analysis of the low-temperature isoclines is continued for the stoichiometric flame systems in Figure 26. The isocline studied in this figure is $T = 1025$ K. This an intermediate enthalpy case as noted in Table 1. The plots in this figure are analogous to those in Figure 25 in terms of line types and other features.

The plots in Figure 26 demonstrate that the agreement between the chemical-kinetic composites and the flame manifolds for the Y_{H_2O}/Y_{OH} projections is generally very good, while the Y_O is often quite different.

The comparison of the two-dimensional manifolds is completed in Figure 27 for the $T = 1025$ K isocline of the rich flame systems at the highest enthalpy. In these plots, there is excellent agreement for Y_{OH} and reasonably good agreement for Y_O.

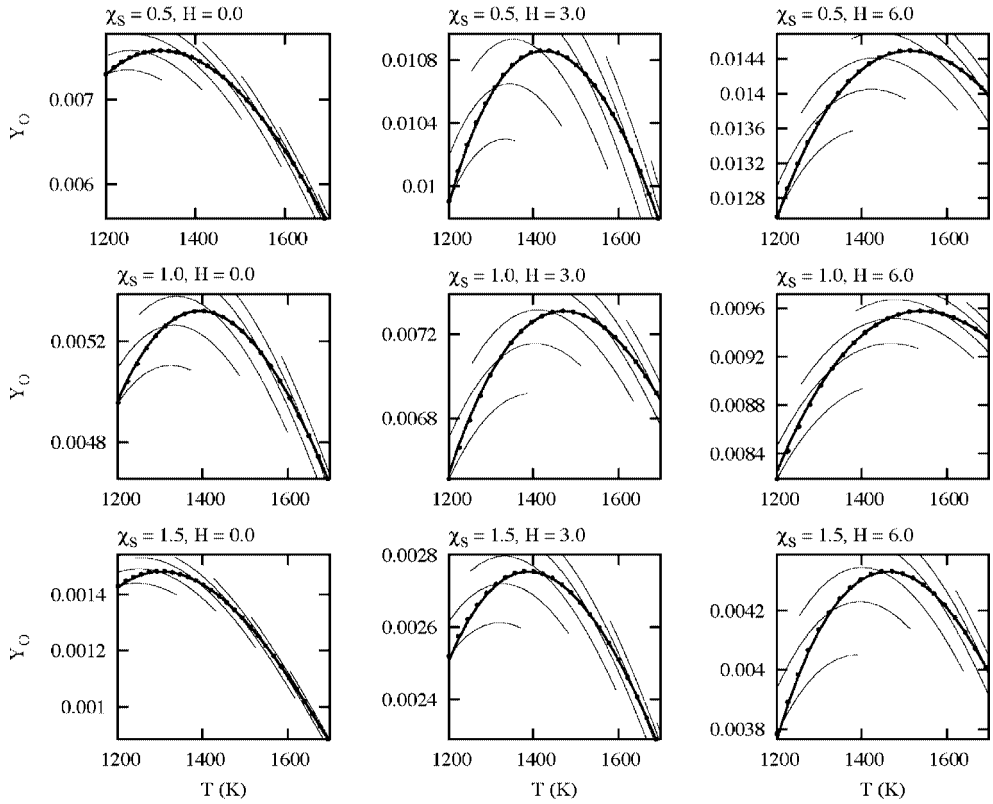

Figure 23. A comparison is made between composite chemical-kinetic manifolds and the flame manifolds in these plots for the nine systems. The description of these plots can be found in Figure 11.

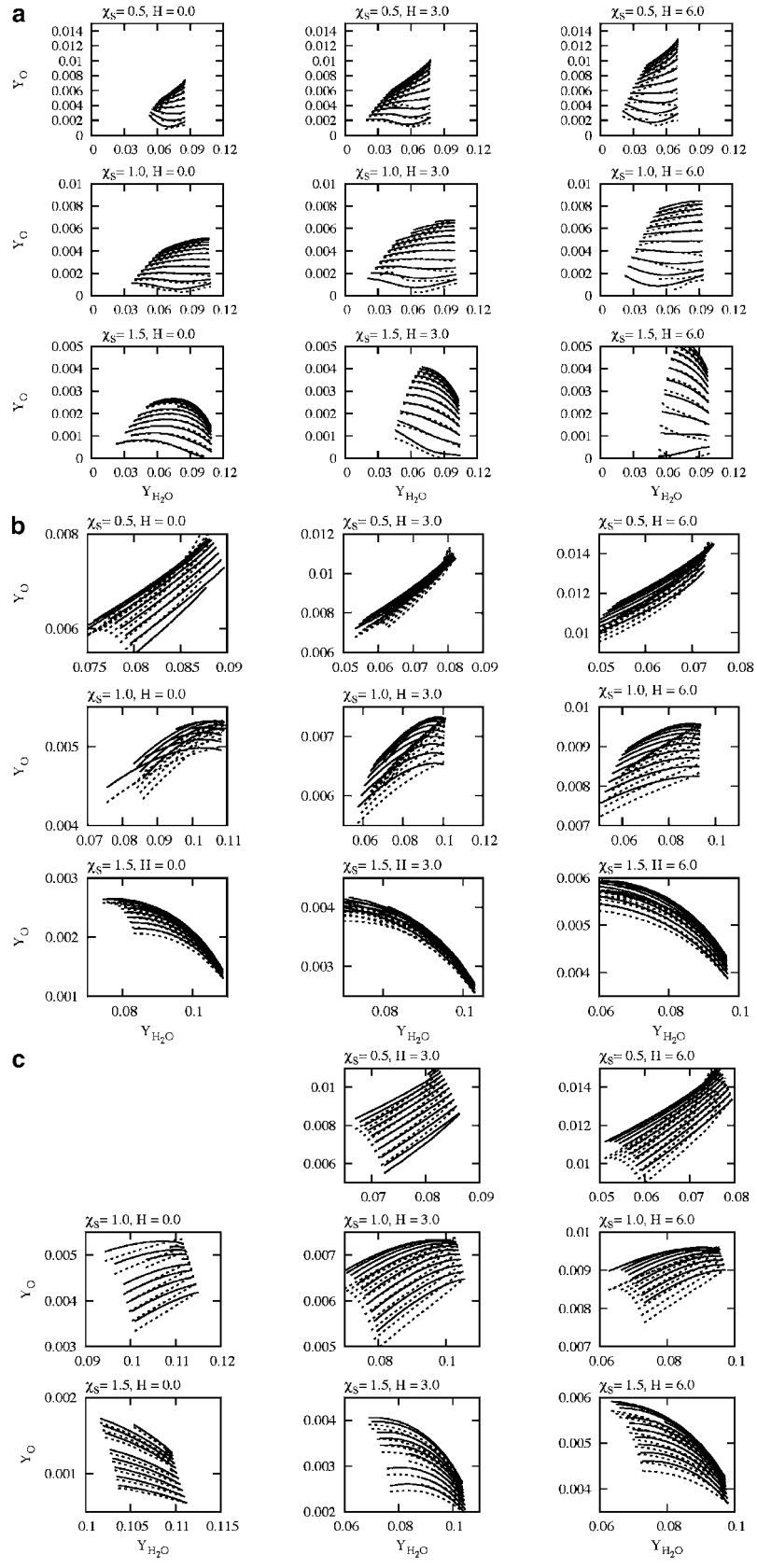

Figure 24. (a) A comparison is made between the two-dimensional flame manifolds (solid lines) and the chemical-kinetic composite manifolds (dashed lines) for the two-dimensional manifolds of the nine systems of Table 1 for the lowest temperature portions of the manifolds of Figure 20. (b) These plots are a continuation of those in (a) for the middle temperature range for the manifolds of Figure 20. (c) These plots complete the comparison of the flame manifolds and the chemical-kinetic composites started in (a) and (b). These plots are for the highest temperature ranges of the manifolds of Figure 20.

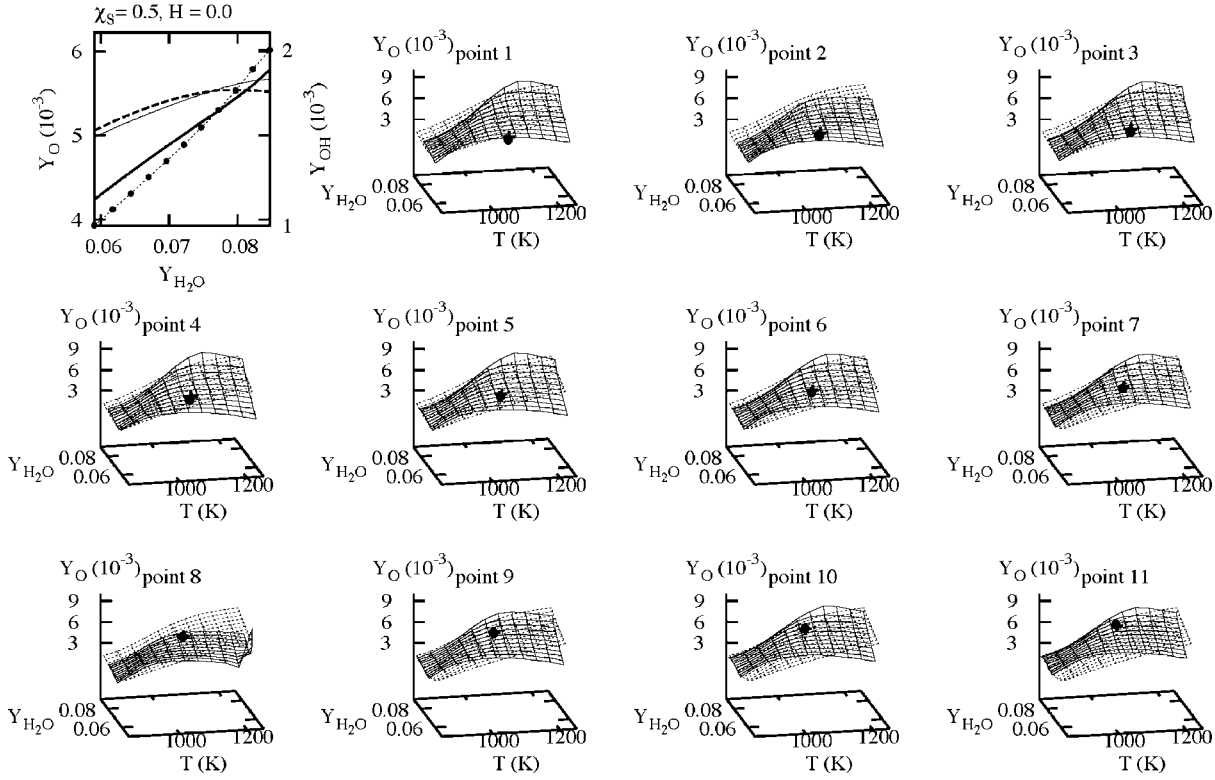

Figure 25. The top left plot shows two projections of a $T = 1050$ K isocline and makes comparisons with the chemical-kinetic composites as described in the text. The other plots show all of the surfaces used to generate the isoclines. The description of these surfaces can be found in the caption to Figure 14.

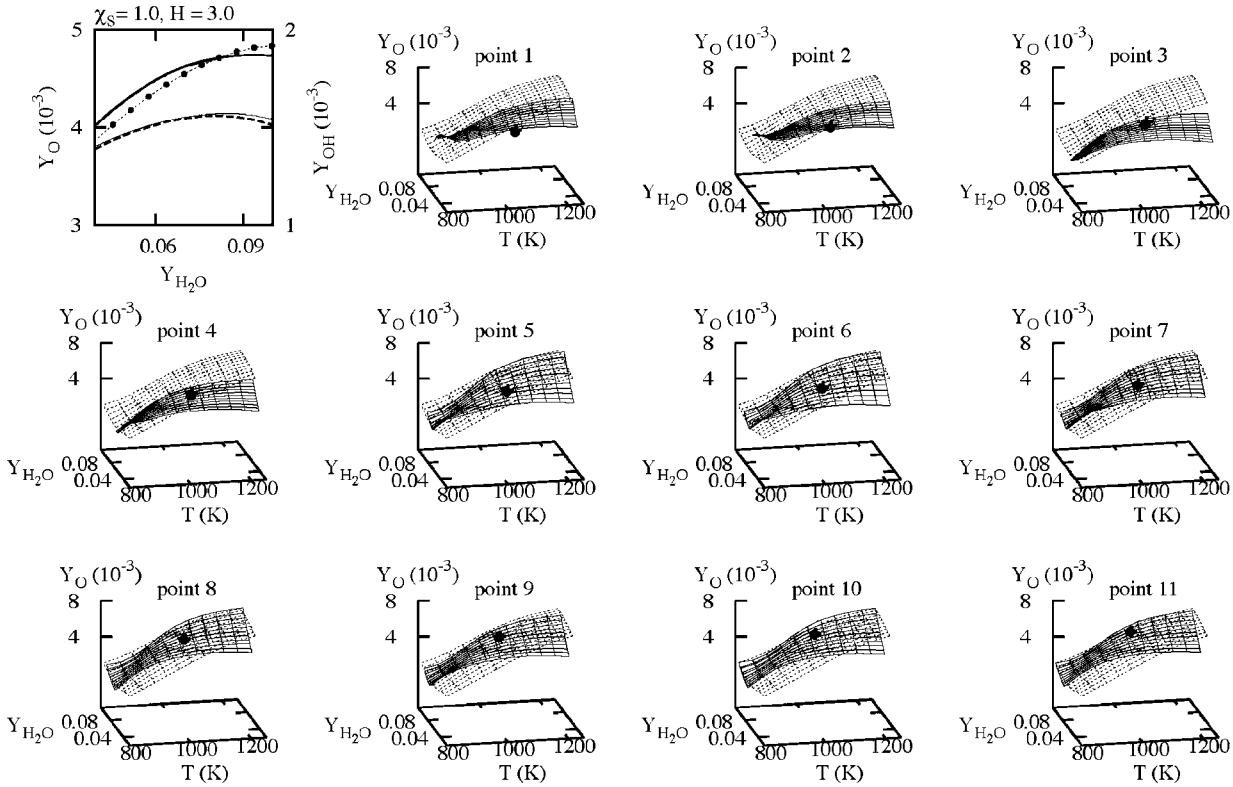

Figure 26. The intermediate-enthalpy stoichiometric flame system is shown here with the plots that are analogous to those in Figure 25.

D. Analysis. The main concern of this Article has been the numerical investigation of low-dimensional manifolds for H_2/O_2 flames and the comparisons of these manifolds to composite manifolds generated from the equivalent adiabatic, isobaric chemical-kinetic system without transport. Because the H_2/O_2 system with multicomponent transport is a fairly complex system, the analysis of the sources of any disparities between the two systems was necessarily qualitative. Future publications will study simpler systems, where detailed analysis is more straightforward to carry out.[39] However, results for one-

dimensional manifolds of simple systems can provide some information about situations that lead to the differences, or lack of differences, noticed in section V.C.

Consider the model reaction−diffusion system:

$$\frac{\partial y_1}{\partial t} = -y_1 + D_1\frac{\partial^2 y_1}{\partial x^2} \tag{5.1a}$$

$$\frac{\partial y_2}{\partial t} = -\gamma y_2 + a y_1^2 + D_2\frac{\partial^2 y_2}{\partial x^2} \tag{5.1b}$$

The steady distribution of this reaction−diffusion system is the solution of the following:

$$0 = -y_1 + D_1\frac{\partial^2 y_1}{\partial x^2} \tag{5.2a}$$

$$0 = -\gamma y_2 + a y_1^2 + D_2\frac{\partial^2 y_2}{\partial x^2} \tag{5.2b}$$

This pair of equations can be converted to a four-dimensional dynamical system, as was done in section III.A of ref 1 for one-dimensional flames. The dynamical system has a two-dimensional stable manifold and a two-dimensional unstable manifold. There is a one-dimensional submanifold of this stable manifold that has the following analytical form:

$$y_2 = \frac{aD_1 y_1^2}{\gamma D_1 - 4D_2} \tag{5.3}$$

The reaction−diffusion manifold can be compared to the one-dimensional manifold of the original system in eq 5.1a without transport:

$$\frac{dy_1}{dt} = -y_1 \tag{5.4a}$$

$$\frac{dy_2}{dt} = -\gamma y_2 + a y_1^2 \tag{5.4b}$$

This system has the following one-dimensional manifold:

$$y_2 = \frac{a}{\gamma - 2} y_1^2 \tag{5.5}$$

Taking the difference between eqs 5.3 and 5.5 gives the error between estimates based on the manifold without diffusion and the actual manifold:

$$\Delta y_2 = y_2^{\mathrm{r}} - y_2^{\mathrm{c}} = \frac{a}{\gamma - 2} y_1^2\left(\frac{\gamma - 2}{\gamma - 4\varphi} - 1\right), \varphi = \frac{D_2}{D_1} \tag{5.6}$$

The relative error is defined as:

$$E_{\mathrm{rel}} \equiv \frac{\Delta y_2}{y_2^{\mathrm{c}}} = \frac{4\varphi - 2}{\gamma - 4\varphi} \tag{5.7}$$

Equation 5.6 demonstrates that the absolute error depends on three factors: (1) the curvature, "a", (2) the attractivity of the manifold, "γ", and (3) the relative values of the diffusivities, "ϕ". Equation 5.7 demonstrates that the relative error depends on the last two of these. The effect of differential diffusion and curvature has been studied previously. For example, ref 22 shows they contribute to changes in a manifold when diffusion is added to chemical reaction in transient reaction−diffusion systems. However, ref 22 did not discuss the role of the degree of attraction of a manifold on the differences between chemical-kinetic manifolds with and without transport. It will be interesting to observe if the effect of attraction observed for the steady problem in this section is also present in the transient case.

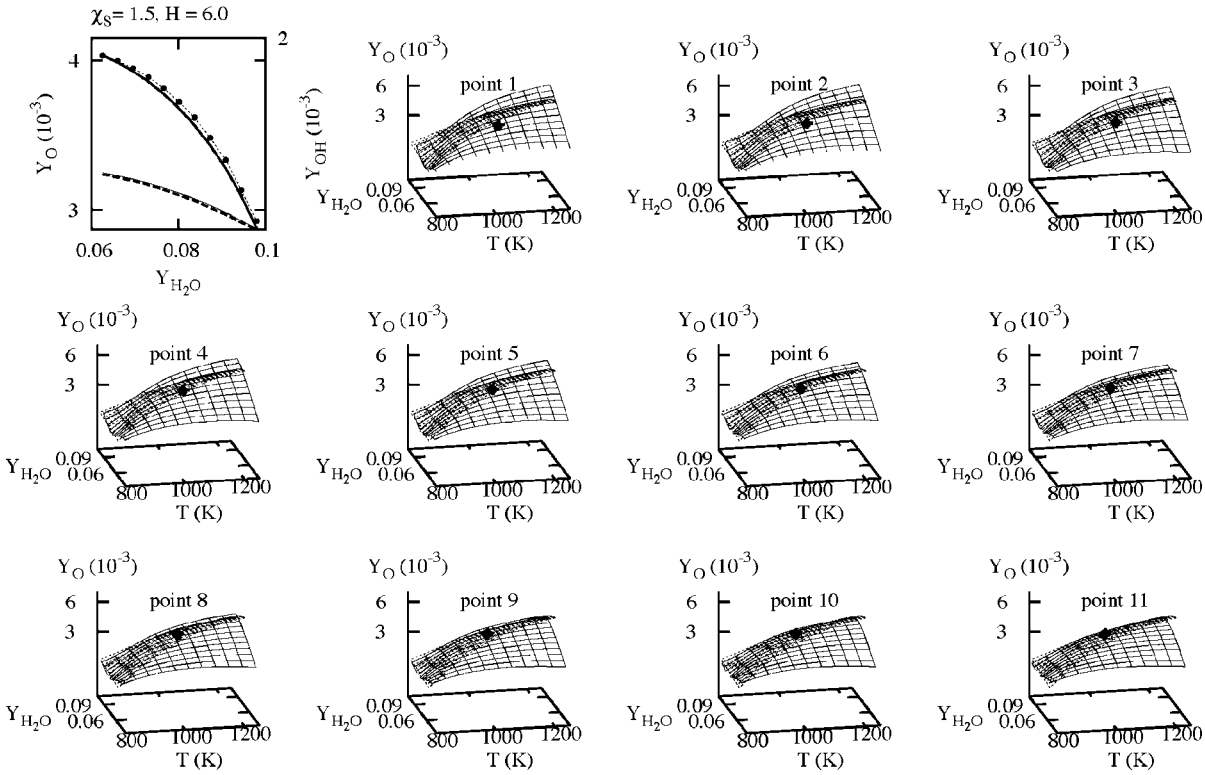

Figure 27. These plots are for a $T = 1025$ K isocline in a rich flame with the highest enthalpy studied (Table 1). The plots are analogous to those in Figures 25 and 26.

A detailed analysis of the differences between the chemical-kinetic composite manifolds and the flame manifolds based on the information gleaned from eqs 5.6 and 5.7, including the role of the differences in transport properties, is left for future work. However, one feature of eqs 5.6 and 5.7 can be directly related to the results in section V.C, and we focus on that here. These equations show that the error is very small if the manifold is "stiff" enough, that is, γ is large enough. The quantities α_1 and α_2 in Table 1 are directly analogous to γ. Table 1 demonstrated that the one-dimensional manifolds were very attractive for all of the systems studied there based on α_1, and the results in section V.C showed that the chemical-kinetic composites were generally in very good agreement with the flame manifolds, consistent with this analysis. On the other hand, Table 1 demonstrated that the two-dimensional manifolds are not very attractive based on α_2. This is consistent with the significant disagreements between the flame versions of the two-dimensional manifold and the chemical-kinetic composites. The cases with the closest values were the rich flames, whose two-dimensional manifolds are the most attractive, also in agreement with this qualitative analysis.

VI. Conclusion

This Article has presented a numerical investigation of the nature of one- and two-dimensional manifolds for one-dimensional premixed flame systems whose dynamics were studied in part 1 (our previous Article).[1] These dynamical systems are based on the work of refs 2 and 3 and treat the flames as initial value problems, rather than the more common approach of boundary value treatments.[33]

Reference 1 demonstrated that steady one-dimensional flames are trajectories on the stable manifold of a saddle fixed point. The saddle fixed point is an equilibrium point of an adiabatic isobaric chemical-kinetic system, but becomes a saddlepoint due to transport processes. In almost all situations studied in ref 1, the dimension of the stable manifold was the same as the dimension of the chemical kinetics system, six. Numerical evidence was presented in ref 1 that there were lower dimensional submanifolds on the stable manifolds that tended to attract trajectories on the stable manifold as they approach the saddlepoint. The current Article has extended these results by explicitly generating one- and two-dimensional manifolds for the flame system.

The primary method of generating the manifolds was a modification of the method proposed in ref 15 (see also ref 17), which is a modification of the method developed by Fraser, Roussel, and co-workers.[7−10] The main modifications to the method were the use of linear systems to make first guesses and a double relaxation method to ensure convergence. For one-dimensional manifolds, a careful examination of the convergence of the manifolds was undertaken. For two-dimensional manifolds, a flexible algorithm for changing the extent of the manifolds was used. Sparse direct linear techniques[36,37] were implemented for two-dimensional manifolds to speed up the relaxation process.

Numerical tests of these low-dimensional manifolds showed that trajectories on the higher dimensional stable manifold were attracted to them (Figure 2) and trajectories started on them remained on them (Figure 3), establishing their invariance. The relaxed manifolds were compared to manifolds generated via an ILDM[6] algorithm. For one-dimensional manifolds, there was good agreement between the ILDM estimates and the relaxed one-dimensional manifolds, but for two-dimensional manifolds there were some significant disagreements. The disagreements are consistent with the fact that two-dimensional manifolds are much less attractive than their one-dimensional counterparts, and it has been found that under these circumstances there can be errors in the ILDM estimates.[15,26]

Section IV of the Article developed prescriptions for comparing the flame manifolds with a collection of appropriate chemical-kinetic manifolds. These comparisons are presented in Figures 11–14 and were made between flame manifolds calculated with the accurate relaxation-iteration algorithm of section II.B and the chemical-kinetic composites calculated in the same manner. It was demonstrated that for one-dimensional manifolds there was excellent agreement between the flame manifold and the chemical-kinetic composites. However, for two-dimensional manifolds, there were some significant disagreements between the flame manifold and the chemical-kinetic composite. Section IV also made some interesting comparisons between composite manifolds generated from the ILDM algorithm and the iterated-relaxed flame manifolds. It was found that while the ILDMs did not accurately model the flame manifolds, chemical-kinetic composites generated with ILDM algorithm were much more accurate (Figures 15–17).

All of the results generated in sections II−IV were for a specific flame system. This was broadened out in section V to the study of nine systems that span a range of stoichiometries and enthalpies. It was demonstrated that these systems possessed attractive one- and two-dimensional manifolds. It was also demonstrated that the one-dimensional manifolds converged down to about 1200 K for all flames studied. It was also shown that two-dimensional manifolds had boundaries that varied considerably among the systems and in general tended to get narrow as the saddlepoint was approached.

In section V, it was also found for these cases that there was good agreement between the ILDM manifolds and the more exact relaxed manifolds for one-dimensional manifolds. However, for two-dimensional manifolds, ILDM estimates were significantly different from those of the relaxed manifolds. These differences can be understood qualitatively by the fact that, unlike the one-dimensional manifolds, the two-dimensional manifolds are not very attractive, and it has been found in the past that these are most likely to show errors in the ILDM estimates of the manifold.[15,26]

Section V.C also had further comparisons between the iterated flame manifolds and composite chemical-kinetic manifolds generated in the same manner. The results in this subsection were consistent with the experience of section IV. For one-dimensional manifolds, there was good agreement between flame manifolds and chemical-kinetic composite manifolds, with some small differences near the low-temperature end of the manifolds. For two-dimensional manifolds, the agreement was worse, with the lean flame examples showing the greatest discrepancies.

Some additional analysis of the reasons for the observations comparing the flame manifolds and chemical-kinetic composites was made at the end of section V, where results for an analytical model were presented. This model suggested that those cases that were most stiff (attractive) were most likely to have chemical-kinetic composites that matched flame manifolds. Because the one-dimensional manifolds are much stiffer than the two-dimensional manifolds, it was suggested in section V that this was the reason that two-dimensional manifolds had the disparities observed. The stiffest case of two-dimensional manifolds studied was the lean flame of Table 1 at low enthalpy, and this case had the best agreement between chemical-kinetic composites and the flame manifolds.

It would be interesting to study the relationship between the chemical-kinetic composites and the flame manifolds with a more detailed examination of transport properties, which the analysis of section V.D suggested would be illuminating. Reference 39 will study smaller systems and will develop further tools for studying the manifolds of flames and their relationship to chemical-kinetic manifolds. It is expected that some of these techniques will be adapted to the study of flame systems such as the ones investigated here and in ref 1.

Acknowledgment. This work was supported by the Office of Basic Energy Sciences, Division of Chemical Sciences, Geosciences, and Biosciences, U.S. Department of Energy, under Contract No. DE-AC02-06CH11357. A.S.T. was also supported by a Maria Goeppert Mayer Distinguished Scholarship at Argonne National Laboratory.

References and Notes

(1) Davis, M. J.; Tomlin, A. S. *J. Phys. Chem. A* **2008**, *112*, 7768.

(2) For example: Hirschfelder, J. O.; Curtiss, C. F. *Adv. Chem. Phys.* **1961**, *3*, 59.

(3) For example: Dixon-Lewis, G. *Proc. R. Soc.* **1968**, *A307*, 111.

(4) For example: Oran, E. S.; Boris, J. P. *Numerical Simulation of Reactive Flows*; Cambridge University Press: Cambridge, 2001. Warnatz, J.; Maas, U.; Dibble, R. W. *Combustion*; Springer: New York, 2001. Kee, R. J.; Coltrin, M. E.; Glarborg, P. *Chemical Reacting Flow: Theory and Practice*; Wiley-Interscience: New York, 2003.

(5) Griffiths, J. F. *Prog. Energy Combust. Sci.* **1995**, *21*, 25. Tomlin, A. S.; Turányi, T.; Pilling, M. J. *Comput. Chem. Kinet.* **1997**, *35*, 293. Okino, M. S.; Mavrovouniotis, M. L. *Chem. Rev.* **1998**, *98*, 243.

(6) Maas, U.; Pope, S. B. *Combust. Flame* **1992**, *88*, 239; *Proc. Combust. Inst.* **1992**, *28*, 103.

(7) Fraser, S. J. *J. Chem. Phys.* **1988**, *88*, 4732.

(8) Roussel, M. R.; Fraser, S. J. *J. Chem. Phys.* **1990**, *93*, 1072. Roussel, M. R.; Fraser, S. J. *J. Chem. Phys.* **1991**, *94*, 7106. Roussel, M. R.; Fraser, S. J. *J. Phys. Chem.* **1991**, *95*, 8762. Roussel, M. R.; Fraser, S. J. *J. Phys. Chem.* **1993**, *97*, 8316; **1994**, *98*, 5174 (E). Fraser, S. J.; Roussel, M. R. *Can. J. Chem.* **1994**, *72*, 800. Fraser, S. J. *J. Chem. Phys.* **1998**, *109*, 411.

(9) Nguyen, A. H.; Fraser, S. J. *J. Chem. Phys.* **1989**, *91*, 186. Roussel, M. R. *J. Math. Chem.* **1997**, *21*, 385. Roussel, M. R.; Fraser, S. J. *Chaos* **2001**, *11*, 196.

(10) Roussel, M. R. A Rigorous Approach to Steady-State Kinetics Applied to Simple Enzyme Mechanisms. Ph.D. Thesis, University of Toronto, 1994.

(11) Lam, S. H.; Goussis, D. A. *Int. J. Chem. Kinet.* **1994**, *26*, 461. For recent developments and important applications, see, for example: Valorani, M.; Najm, H. N.; Goussis, D. A. *Combust. Flame* **2003**, *134*, 35, and references cited therein.

(12) Maas, U.; Pope, S. B. *Proc. Combust. Inst.* **1994**, *25*, 1349.

(13) Yannacopoulos, A. N.; Tomlin, A. S.; Brindley, J.; Merkin, J. H.; Pilling, M. J. *Physica D* **1994**, *83*, 421.

(14) Hadjinicolaou, M.; Goussis, D. A. *SIAM J. Sci. Comput.* **1999**, *20*, 781.

(15) Davis, M. J.; Skodje, R. T. *J. Chem. Phys.* **1999**, *111*, 859.

(16) Skodje, R. T.; Davis, M. J. *J. Phys. Chem. A* **2001**, *105*, 10356.

(17) Nafe, J.; Maas, U. *Combust. Theory Modell.* **2002**, *6*, 697.

(18) Singh, S.; Powers, J. M.; Paolucci, S. *J. Chem. Phys.* **2002**, *117*, 1482.

(19) Bongers, H.; Van Oijen, J. A.; De Goey, L. P. H. *Proc. Combust. Inst.* **2002**, *29*, 1371.

(20) Ren, Z. Y.; Pope, S. B.; Vladimirsky, A.; Guckenheimer, J. M. *J. Chem. Phys.* **2006**, *124*, 11411.

(21) Goussis, D. A.; Valorani, M.; Creta, F.; Najm, H. N. *Prog. Comp. Fluid Dyn.* **2005**, *5*, 316.

(22) Ren, Z. Y.; Pope, S. B. *Combust. Flame* **2006**, *147*, 243.

(23) (a) Davis, M. J. *J. Phys. Chem. A* **2006**, *110*, 5235. (b) Davis, M. J. *J. Phys. Chem. A* **2006**, *110*, 5257.

(24) Roussel, M. R.; Tang, T. *J. Chem. Phys.* **2006**, *125*, 214103.

(25) Bykov, V.; Maas, U. *Combust. Theory Modell.* **2007**, to be published.

(26) Kaper, H. J.; Kaper, T. J. *Physica D* **2002**, *165*, 66.

(27) Zagaris, A.; Kaper, H. G.; Kaper, T. J. *Multiscale Model. Simul.* **2004**, *2*, 613; *Math. Nach.* **2005**, *278*, 1629.

(28) Gorban, A. N.; Karlin, I. V.; Zinovyev, A. Y. *Physica A* **2004**, *333*, 106; *Phys. Rep.* **2004**, *396*, 197.

(29) Lam, S. H. *Combust. Sci. Technol.* **2007**, *179*, 767.

(30) O Conaire, M.; Curran, H. J.; Simmie, J. M.; Pitz, W. J.; Westbrook, C. K. *Int. J. Chem. Kinet.* **2004**, *36*, 603.

(31) See, for example: Seydel, R. *From Equilibrium to Chaos: Practical Bifurcation and Stability Analysis*; Elsevier: New York, NY, 1988.

(32) Smooke, M. D. *J. Comput. Phys.* **1982**, *48*, 72.

(33) Kee, R. J.; Grcar, J. F.; Smooke, M. D.; Miller, J. A. A Fortran Program for Modeling Steady Laminar One-Dimensional Flames, SAND85-8240, Sandia National Laboratories, 1985.

(34) Kelley, C. T. *Solving Nonlinear Equations with Newton's Method (Fundamentals of Algorithms)*; SIAM: Philadelphia, PA, 1987.

(35) Anderson, E.; Bai, Z.; Bischof, C.; Blackford, S.; Demmel, J.; Dongarra, J.; Du Croz, J.; Greenbaum, A.; Hammarling, A.; McKerney, A.; Sorensen, D. *LAPACK Users' Guide*, 3rd ed.; SIAM: Philadelphia, PA, 1999.

(36) Duff, I. S.; Erisman, A. M.; Reid, J. K. *Direct Methods for Sparse Matrices*; Clarendon: Oxford, 1986.

(37) Demmel, J. W.; Eisenstat, S. C.; Gilbert, J. R.; Li, X. S.; Liu, J. W. H. *SIAM J. Matrix Anal. Appl.* **1999**, *20*, 720.

(38) Perko, L. *Differential Equations and Dynamical Systems*; Springer-Verlag: New York, NY, 1996.

(39) Davis, M. J.; Zagaris, A.; Kaper, T. J.; Tomlin, A. S., to be submitted.

JP801370P